JRC Scientific and Technical Reports

Impact of Pseudolite Signals on Non-Participating GNSS Receivers

Modelling Receiver Losses

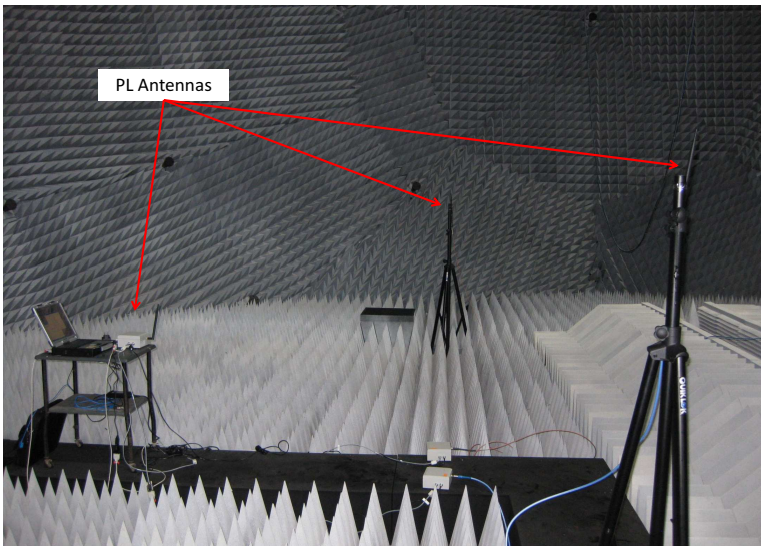

D. Borio, C. O'Driscoll, J. Fortuny

EUR xxxxx EN - 2011

JRC
EUROPEAN COMMISSION

ipsc
Institute for the Protection and Security of the Citizen

The mission of the JRC-IPSC is to provide research results and to support EU policy-makers in their effort towards global security and towards protection of European citizens from accidents, deliberate attacks, fraud and illegal actions against EU policies.

European Commission
Joint Research Centre
Institute for the Protection and Security of the Citizen

Contact information
Address: Via E. Fermi, 2749, I-21027 Ispra (VA), Italy
E-mail: joaquim.fortuny@jrc.ec.europa.eu
Tel.: +39 0332 785104
Fax: +39 0332 785469

http://ipsc.jrc.ec.europa.eu/
http://www.jrc.ec.europa.eu/

JRC []
EUR xxxxx EN
ISBN X-XXXX-XXXX-X
ISSN 1018-5593
DOI XXXXX

Luxembourg: Office for Official Publications of the European Commission

Printed in Italy

Contents

List of Figures

List of Tables

1 Introduction

Pseudo-satellites or pseudolites are ground based-transmitters intended for location applications. More specifically, pseudolites are expected to play the role of Global Navigation Satellite System (GNSS) satellites when GNSS signals are not available or do not provide sufficient coverage for the considered application. GNSS signals can be easily blocked by walls and other obstacles, thus GNSS location can be challenging in harsh environments such as indoors. Pseudolites have the potential to bridge the gap between outdoor and indoor location. The use of this technology is not however limited to indoor navigation but finds several applications [2] such as improving the GNSS satellite geometry for landing applications, precise farming, machine control and others.
Despite their potential, the deployment of pseudolites involves several issues [3] including regulatory aspects, interference problems and monitoring implications. More specifically, compatibility between existing GNSS receivers and pseudolite signals is considered a relevant point to account for. In order to limit hardware changes in existing GNSS receivers, it has been proposed to broadcast pseudolite signals in the GNSS bands. In this way, it will be possible to process pseudolite signals using existing GNSS receivers at the cost of small firmware updates. Broadcasting pseudolite signals in the GNSS bands inevitably causes interference problems: it is feared that pseudolite signals can jam the much weaker GNSS signals most of all in legacy receivers not designed to handle pseudolite signals. This kind of receivers are denoted as non-participating.
In order to assess the potential impact of pseudolite on existing GNSS receivers, the S40 working group of European Conference of Postal and Telecommunications Administrations (CEPT) prepared a preliminary report [4] addressing problems such as spectrum overlap and pseudolite interfering power. However, the report did not considered modulation aspects specific to GNSS and pseudolite signals and additional work was required to better investigate compatibility issues between these two technologies.
The European Commission (EC) Joint Research Centre of the European Commission (JRC) has been involved in the coexistence analysis between pseudolites and GNSS since September 2010. The research activities of JRC on this subjects have been coordinated with CEPT's efforts with the goal of better characterizing and understanding potentially harmful interactions between pseudolites and GNSS. Research at the JRC has lead to the publications of two technical reports:

- **pseudolite impact on non-participating receivers** [5]: conducted mode experiments have been used to determine the impact of pseudolite signals on commercial receivers. Degradations in terms of signal quality (Carrier-to-Noise density power ratio (C/N_0)) and in the position domain have been reported as a function of the different pseudolite signal parameters;
- **pseudolite scoping study** [3]: a review of the different pseudolite technologies and the associated issues has been provided.

In the first report, an experimental approach has been used to determine the impact of pseudolites on commercial Global Positioning System (GPS) receivers. However limited analytical results were provided and no insight was provided on the mechanisms that lead to losses in a non-participating receiver.

In this report the preliminary analysis presented in [5] is significantly expanded and a theoretical model able to approximately predict the loss caused by a pseudolite is developed. The analysis provides insight on the different mechanisms that lead to receiver losses. Although specific focus is given to pulsed pseudolite signals, the analysis is general and the effect of frequency offsets with respect to GNSS frequency bands can be easily accounted for. The case of continuous pseudolite signal can be obtained by setting the pulse duty cycle to 1 (the pulse is always on).
Theoretical findings are supported by experiments conducted using commercial receivers. In this case, real pseudolites provided by Space System Finland (SSF) have been used along with a Spirent GSS8000, a GNSS constellation simulator able to generate both GPS and Galileo signals. All the experiments were run in radiated-mode inside the JRC anechoic chamber.
The parameters of the proposed theoretical model have been tuned using the experimental findings and the resulting model have been used to determine the minimum distance that should separate a pseudolite from a non-participating receiver. This distance has been determined in order to guarantee

a maximum C/N_0 loss and has been computed for different pseudolite transmitted power levels.

This report is intended as a contribution to CEPT activities on pseudolite compatibility analysis and it is organized as follows. Section 2 introduces the signal models and briefly summarizes the operations performed by a non-participating GNSS receiver. An analytical model for the loss caused by a pseudolite signal on non-participating receivers is developed in Section 3 whereas experimental results and their agreement with the proposed analytical model are discussed in Section 4. In Section 5, the results obtained in Section 3 and Section 4 are finally used to determined the minimum distance and maximum duty cycle leading to a predefined loss. Conclusions and recommendations are provided in Section 6.

2 Signal and System Model

The signal at the input of a GNSS receiver in a one-path additive Gaussian channel and in the presence of pseudolite signals can be modeled as

$$r(t) = \sum_{l=0}^{L-1} y_l(t) + \sum_{j=0}^{J-1} y_{p,j}(t) p_j(t) + \eta(t) \tag{1}$$

which is the sum of L useful signals transmitted by L different satellites, J pseudolite signals, and a noise term, $\eta(t)$.
Each useful signal, $y_l(t)$ can be expressed as

$$y_l(t) = \sqrt{2C_l} d_l\left(t - \tau_{0,l}\right) c_l\left(t - \tau_{0,l}\right) \cos\left(2\pi(f_{RF} + f_{d,l})t + \varphi_{0,l}\right) \tag{2}$$

where

- C_l is the power of the lth useful signal;
- $d_l(\cdot)$ is the navigation message;
- $c_l(\cdot)$ is the lth ranging sequence extracted from a family of quasi-orthogonal codes and used for spreading the signal spectrum
- $\tau_{0,l}$, $f_{d,l}$ and $\varphi_{0,l}$ are the delay, Doppler frequency and phase introduced by the communication channel
- f_{RF} is the centre frequency of the GNSS signal.

In (1), the following model has been used to describe the jth pseudolite signal

$$y_{p,j}(t) = y_{p,j}(t) p_j(t) \tag{3}$$

which is the product of two terms:

- $y_{p,j}(t)$ is a continuous signal that assumes the same form as (2)
- $p_j(t)$ is a binary sequence assuming values in $\{0, 1\}$ defining a pulsing sequence.

$p_j(t)$ defines the time instants when the pseudolite signal is effectively transmitted. The choice of this pseudolite signal format is common in the literature [2, 6] and allows a unified analytical treatment of both pulsed and continuous pseudolite signals. More specifically, when

$$p_j(t) = 1 \tag{4}$$

(3) degenerates to the case of continuous pseudolite signals. The pulsing scheme, $p_j(t)$, has been introduced as an effective technique for reducing interference problems [2] with non-participating receivers and its impact on non-participating GNSS receivers will be evaluated in the remainder of this document. It is noted that (3) implicitly assumes that the pseudolite signal has the same centre frequency of useful GNSS signals. In this report the impact of a frequency offset between the two types of signals is not considered and left for future analysis.
The ranging sequence, $c_l(\cdot)$, is usually made of several components that include primary and secondary spreading codes and a subcarrier. More specifically

$$c_l(t) = \sum_{k=-\infty}^{+\infty} r_l[k] g(t - kT_{sb}) \tag{5}$$

where

- $r_l[k]$ is a pseudo-random sequence given by the combination of the primary and secondary spreading codes

- $g(t)$ is the subcarrier that defines the spectral characteristics of the GNSS signal
- T_{sb} is the subcarrier or chip duration.

Several modulations have be adopted by the different GNSS. The most common one is binary phase shift keying (BPSK), which has been widely used by legacy GNSS signals. When a BPSK modulation is adopted then

$$g_{BPSK}(t) = \begin{cases} 1 & \text{for } 0 \leq t < T_{sb} \\ 0 & \text{otherwise} \end{cases}. \tag{6}$$

In new and modernized GNSS the binary offset carrier (BOC) modulation has been introduced [7]. In its basic form, the BOC subcarrier is defined as [1]

$$g_{BOC}(t) = \begin{cases} \text{sign}\left(\sin(2\pi f_{sb} t)\right) & \text{for } 0 \leq t < T_{sb} \\ 0 & \text{otherwise} \end{cases}. \tag{7}$$

where

$$\text{sign}(t) = \begin{cases} 1 & t > 0 \\ -1 & t < 0 \end{cases} \tag{8}$$

and f_{sb} is the subcarrier frequency. Eq. (7) defines the sine-BOC subcarrier and several variants exists for this type of modulation [1]. It is noted that the GNSS and pseudolite signals may have different subcarrier thus leading different interference impacts.
Due to the quasi-orthogonality of the spreading codes, a GNSS receiver is able to process the L useful signals independently. More specifically, a single signal is selected at a time through a correlation/despreading process. It is noted that residual components from other signals can be present leading to Multiple Access Interference (MAI). This issue is not addressed in this report and a single GNSS signal is considered.
In addition to this, the case of a single pseudolite signal is at first considered and (1) becomes

$$r(t) = y(t) + y_p(t)p(t) + \eta(t) \tag{9}$$

where the indexes, l and j have been dropped for ease of notation.

2.1 GNSS Receiver Operations

Signal (9) is filtered and down-converted by the receiver front-end before being digitized. Digitization implies two different operations: sampling and amplitude quantization. In the following, sampling and quantization are considered separately. In addition, it is assumed that the signal is sampled without introducing significant distortions. After down-conversion and sampling (9) becomes:

$$r_{IF}[n] = y_{IF}(nT_s) + y_{p,IF}(nT_s)p(nT_s) + \eta_{IF}(nT_s) = y_{IF}[n] + y_{p,IF}[n]p[n] + \eta_{IF}[n] \tag{10}$$

where the notation $x[n]$ is used to denote a discrete time sequence sampled at the frequency $f_s = \frac{1}{T_s}$. The index "IF" is used to denote a signal down-converted to an intermediate frequency, f_{IF}. In (10),

$$y_{IF}[n] = \sqrt{2C}d\left(nT_s - \tau_0\right)c\left(nT_s - \tau_0\right)\cos\left(2\pi\left(f_{IF} + f_0\right)nT_s + \varphi_0\right) \tag{11}$$

and

$$y_{p,IF}[n] = \sqrt{2C_p}d_p\left(nT_s - \tau_p\right)c_p\left(nT_s - \tau_p\right)\cos\left(2\pi\left(f_{IF} + f_p\right)nT_s + \varphi_p\right) \tag{12}$$

where the subscript "p" is used to denote quantities relative to the pseudolite signal. The noise term, $\eta_{IF}[n]$, is assumed to be a white additive Gaussian noise with variance σ^2_{IF}. σ^2_{IF} depends on the filtering, down-conversion and sampling strategy applied by the receiver front-end. A convenient choice is to assume $\sigma^2_{IF} = N_0 B_{IF}/2$ where B_{IF} is the front-end bandwidth and N_0 is the power spectral density of the input noise $\eta(t)$. The ratio between the carrier power, C, and the noise power spectral density, N_0, defines the Carrier-to-Noise density power ratio, C/N_0, one of the main signal quality indicators used in GNSS.

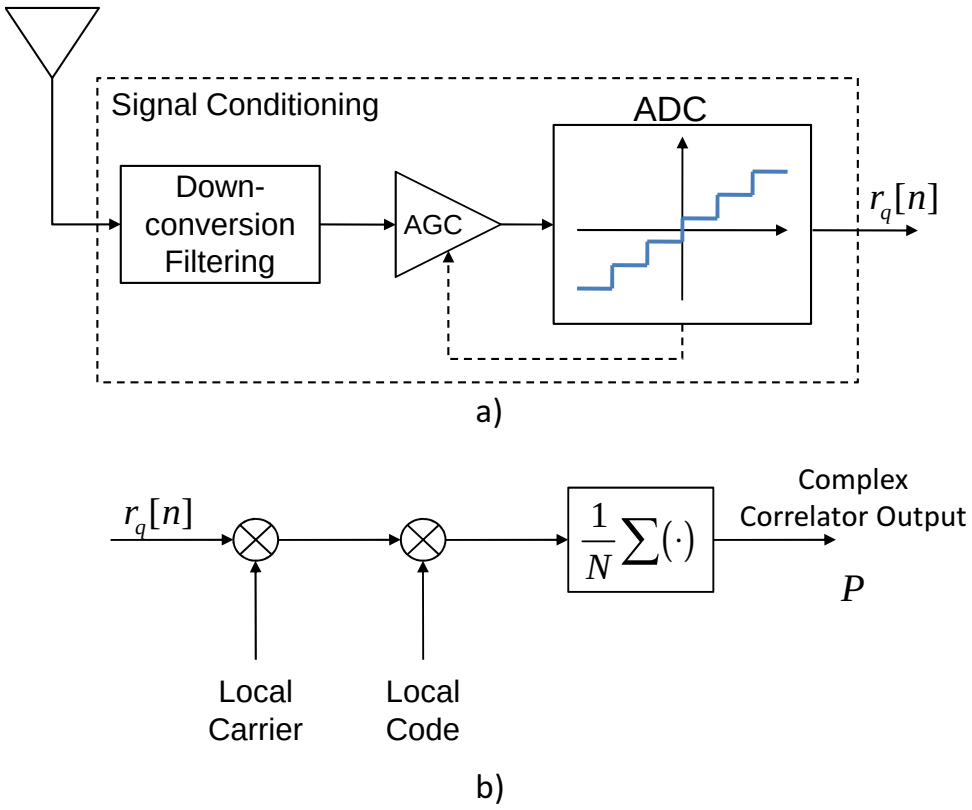

Figure 1: Basic operations performed by a GNSS receiver. a) Signal conditioning: the RF analog signal is converted into an IF digital sequence. b) The correlation process.

The amplitude quantization process is shown in the upper part of Fig. 1 and consists of a scaling, introduced by the Automatic Gain Control (AGC), and a mapping of the continuous values of $y_{IF}[n]$ into a finite discrete alphabet. This second operation is performed by the Analog to Digital Converter (ADC). In this paper, ideal and very slow AGCs are considered. Definitions of different AGC types are provided by [2] and the considered cases are characterized by constant AGC gains. An ideal AGC ignores the pseudolite pulse and provides a gain independent from the pseudolite power. In the very slow case, the pseudolite power impacts the selection of the gain that is fixed according to the total power measured by the AGC. The case of a simple uniform quantizer is considered and it is assumed that the pseudolite power is sufficiently high to saturate the ADC.
Under these conditions, the signal at the output of the ADC can be modeled as:

$$r_q[n] = Q_B(A_g(y_{IF}[n] + A_g y_{p,IF}[n]p[n] + \eta_{IF}[n])) \tag{13}$$

where

- $Q_B(\cdot)$ is the quantization function adopted by an ADC employing B bits for the signal representation. In a uniform quantizer, $Q_B(\cdot)$ is a symmetric stair-case function producing output values in the set $\left\{-2^B+1, -2^B+3, ..., -1, 1, ..., 2^B-3, 2^B-1\right\}$;
- A_g is the AGC gain.

The impact of the quantization function $Q_B(\cdot)$ depends on the gain provided by the AGC and by the ADC operation mode. Thus different operating conditions will be considered in Section 3 leading to two different pseudolite losses.

After signal conditioning, the sequence $r_q[n]$ is correlated with local replicas of the signal code and carrier. This process is shown in the lower part of Fig. 1 and a complex correlator output is computed

as

$$P = \frac{1}{N}\sum_{n=0}^{N-1} r_q[n]c\left(nT_s - \tau\right)\exp\left\{-j2\pi(f_{IF} + f_d)nT_s - j\varphi\right\} \tag{14}$$

where τ, f_d and φ are the code delay, the Doppler frequency and the phase tested by the receiver. N is the number of samples used for computing a correlator output and $T_c = NT_s$ is the coherent integraton time. It is noted that the computation of correlator outputs is essential for the proper functioning of a GNSS receiver and they are used both in acquisition and tracking [8], the main receiver operating modes. Thus, the quality of a GNSS signal can be defined after correlation as [9, 10]:

$$SNR_{out} = \max_{\tau, f_d, \varphi} \frac{|\mathrm{E}\left\{P\right\}|^2}{\frac{1}{2}\mathrm{Var}\left\{P\right\}} \tag{15}$$

where SNR_{out} is the coherent output signal to noise ratio (SNR). The factor $1/2$ in (15) accounts for the fact that P is a complex quantity and only the variance of its real part is considered. The loss experienced at the correlator output due to the presence of a strong pulsed pseudolite signal is determined as the ratio between the measured SNR and the ideal coherent output SNR determined in the absence of quantization and interference.

3 Loss Model

In this section, a theoretical model for the evaluation of the loss caused by a pulsed pseudolite signal is considered. Since, in general, it is not possible to evaluate the coherent output SNR in the presence of pulse interference directly from (13), two limit cases are considered at first. The evaluation of the SNR in close form is prevented by the highly non-linear function, $Q_B(\cdot)$. The considered cases are

- **small signal approximation**: the power of the signals in (13) is small as compared to the noise variance. This allows one to develop a sort of linear approximation of the quantization function $Q_B(\cdot)$. $Q_B(\cdot)$ scales the signals components and introduces additional quantization noise
- **saturation mode**: the pseudolite signal is so powerful to saturate the receiver ADC. This condition should be considered the limit to which the loss converges as the pseudolite signal power goes to infinity.

These two approximations are then combined to form a composite loss model able to quantify (at least approximately) the loss caused by a disturbing pseudolite signal.

3.1 Small Signal Approximation

When the power of the composite signal $y_I F[n] + y_{p,IF}[n]p[n]$ is small as compared to the noise variance $\sigma^2_{IF} = \mathrm{Var}\{\eta_{IF}[n]\}$, it is possible to apply the approach used in [11] to compute the quantization loss caused by the receiver front-end.
More specifically, under the hypothesis

$$\left|\mathrm{E}\left[y_I F[n] + y_{p,IF}[n]p[n]\right]\right|^2 < \sigma^2_{IF} \tag{16}$$

it is possible to show [11] that

$$\mathrm{E}\{r_q[n]\} \approx \frac{a}{\sigma_{IF}}\left[y_I F[n] + y_{p,IF}[n]p[n]\right] \tag{17}$$

where

$$a = \sqrt{\frac{2}{\pi}}\left[1 + 2\sum_{i=1}^{2^{B-1}-1}\exp\left\{-\frac{i^2}{2A_g^2\sigma^2_{IF}}\right\}\right]. \tag{18}$$

In a similar way, the variance of $r_q[n]$ is given by

$$\mathrm{Var}\{r_q[n]\} = b = 1 + 8\sum_{i=0}^{2^{B-1}-1} i\,\mathrm{erfc}\left(\frac{i}{\sqrt{2}A_g\sigma_{IF}}\right). \tag{19}$$

where $\mathrm{erfc}(\cdot)$ denotes the complementary error function. It is noted that the quantity $L_q = \frac{a^2}{b}$ defines the quantization loss obtained in the absence of pseudolite signal.
Thus, under the small signal approximation, $r_q[n]$ can be approximated as

$$r_q[n] \approx \frac{a}{\sigma_{IF}}\left[y_I F[n] + y_{p,IF}[n]p[n]\right] + \eta_q[n] \tag{20}$$

where $\eta_q[n]$ is a zero mean random variable with variance (19). It is note that $\eta_q[n]$ is not Gaussian since it also accounts for the additional noise introduced by the quantization process. It is however possible to show that $\eta_q[n]$ is a white sequence when $\eta_{IF}[n]$ is white [12]. Under the small signal approximation, the AGC/ADC are approximated as a linear device that scales the input useful signals and adds a quantization noise term. Eq. (20) can be used to determine the impact of the pseudolite signal under the small signal approximation. More specifically, the linearity of the correlation process (14) can be used to express the correlator output as

$$P = P_s + P_I + P_\eta \tag{21}$$

that is the sum of three terms, derived from the processing of the useful signal, the pseudolite interferer and the noise component, respectively. More specifically, it is possible to show

$$\begin{aligned} P_s &= \frac{a}{\sigma_{IF}} \mathrm{E}\left[\frac{1}{N}\sum_{n=0}^{N-1} y_I F[n] c\left(nT_s-\tau\right)\exp\left\{-j2\pi(f_{IF}+f_d)nT_s - j\varphi\right\}\right] \\ &= \frac{a}{\sigma_{IF}}\sqrt{\frac{C}{2}}\frac{\sin\left(\pi\Delta f N T_s\right)}{N\sin\left(\pi\Delta f T_s\right)} R_c(\Delta\tau)\exp\left\{j\Delta\varphi\right\} \end{aligned} \tag{22}$$

where

- Δf is the residual Doppler frequency error committed by the receiver. Δf is the difference between the frequencies of the incoming signal and local carrier
- $\Delta\tau$ is the residual delay between incoming local signal and $R_c(\cdot)$ is the autocorrelation function of the ranging code, $c[n]$. The shape of $R_c(\cdot)$ is essentially determined by the subcarrier
- $\Delta\varphi$ is a residual phase error.

Under the assumption of perfect frequency and delay synchronization required for the maximization of (15), (22) becomes

$$\mathrm{E}\left[P_s\right] = \frac{a}{\sigma_{IF}}\sqrt{\frac{C}{2}}\exp\left\{j\Delta\varphi\right\}. \tag{23}$$

The term P_I is given by the correlation of the pseudolite component with the local signal replica:

$$P_I = \frac{a}{\sigma_{IF}}\frac{1}{N}\sum_{n=0}^{N-1} y_{p,IF}[n]p[n]c\left(nT_s-\tau\right)\exp\left\{-j2\pi(f_{IF}+f_d)nT_s - j\varphi\right\}. \tag{24}$$

In the following, $y_{p,IF}[n]p[n]$ is assimilated to a random process and P_I is characterized in terms of mean and variance. More specifically,

$$\begin{aligned} \mathrm{E}\left[P_I\right] &= \frac{a}{\sigma_{IF}}\frac{1}{N}\sum_{n=0}^{N-1}\mathrm{E}\left[y_{p,IF}[n]p[n]\right] c\left(nT_s-\tau\right)\exp\left\{-j2\pi(f_{IF}+f_d)nT_s - j\varphi\right\} \\ &= \frac{a}{\sigma_{IF}}\sqrt{\frac{C_p}{2}} A_{p,c}\left(\delta\tau,\Delta f\right) \end{aligned} \tag{25}$$

where $A_{p,c}\left(\delta\tau,\Delta f\right)$ is the cross-ambiguity function between the pseudolite sequence and the local code $c[n]$. $A_{p,c}\left(\delta\tau,\Delta f\right)$ is a function of the relative delay and frequency between the local and pseudolite codes. It is noted that $y_{p,IF}[n]p[n]$ should be designed to have good cross-correlation properties with respect to the GNSS codes, i.e.,

$$A_{p,c}\left(\delta\tau,\Delta f\right) \approx 0. \tag{26}$$

In the following, it is assumed that P_I is zero mean. This assumption can be violated when the pseudolite signal power is much stronger than that of GNSS signals. In such a case there would be residual terms that could lead to near-far problems potentially leading to biased measurements. In this analysis, only the increase of noise caused by pseudolite signals is considered and P_I is assumed zero mean. Using the properties of random processes through a linear device, it is possible to show that

$$\mathrm{Var}\left\{P_I\right\} = \frac{a^2}{\sigma_{IF}^2}\frac{C_p}{2N}\int_{-0.5}^{0.5} G_{pl}(f)G_c(f)df \tag{27}$$

where

$$G_c(f) = \mathcal{F}\left\{\mathrm{E}\left[c(nT_s-\tau)c(mT_s-\tau)\right]\right\} = \mathcal{F}\left\{R_c\left((n-m)T_s\right)\right\} \tag{28}$$

is the Discrete Time Fourier Transform (DTFT) of the local code correlation function. The shape of $G_c(f)$ essentially depends on the code subcarrier. Close-form expressions for $G_c(f)$ for several modulations

can be found in [1]. Here f denotes digital frequencies (i.e. frequencies normalized with respect to the sampling frequency). In (27),

$$G_{pl}(f) = \mathcal{F}\left\{\mathrm{E}\left[c_p[n]p[n]c_p[m]p[m]\right]\right\} = \mathcal{F}\left\{R_{pl}\left((n-m)T_s\right)\right\} \tag{29}$$

is the spectrum of the $c_p[n]p[n]$. It is noted that $p[n]$ can strongly impact the spectral characteristics of the pseudolite thus the pulsing scheme should be carefully selected in order to preserve the ranging capabilities of the unpulsed signal.
From definitions (28) and (29), it is possible to show the following properties:

$$\int_{-0.5}^{0.5} G_c(f)df = 1 \tag{30}$$

$$\int_{-0.5}^{0.5} G_{pl}(f)df = d. \tag{31}$$

where

$$d = E\left[\frac{1}{N}\sum_{i=0}^{N-1} p[n]\right] \tag{32}$$

is the duty cycle of the pseudolite pulsing scheme.
A normalized pseudolite spectrum can be defined as

$$\bar{G}_{pl}(f) = \frac{1}{d}G_{pl}(f) \tag{33}$$

and (27) assumes the following form:

$$\mathrm{Var}\left\{P_I\right\} = \frac{a^2}{\sigma_{IF}^2}d\frac{C_p}{2N}\int_{-0.5}^{0.5}\bar{G}_{pl}(f)G_c(f)df = a^2 d\frac{C_p}{2\sigma_{IF}^2 N}k_d \tag{34}$$

where

$$k_d = \int_{-0.5}^{0.5}\bar{G}_{pl}(f)G_c(f)df \tag{35}$$

is the equivalent of the Spectral Separation Coefficient (SSC) [10, 9] for digital sequences. More specifically, it is possible to show that for small sampling interval, T_s, the quantity $T_s k_d$ converges to the standard SSC. In the following, it is assumed that the sampling frequency is much larger than the code and pseudolite bandwidths and k_d is replaced by his analog counterpart.
The noise term, $\eta_q[n]$, is zero mean and

$$\begin{aligned}\mathrm{E}\left[P_\eta\right] &= 0\\ \mathrm{Var}\left\{P_\eta\right\} &= \frac{b}{N}.\end{aligned} \tag{36}$$

Using the previous results, the coherent output SNR (15) can be expressed as

$$SNR_{out} = 2\frac{\frac{a^2}{\sigma_{IF}^2}\frac{C}{2}}{\frac{b}{N} + a^2 d\frac{C_p}{2\sigma_{IF}^2 N}k_d} = \frac{CN}{\sigma_{IF}^2}L_q\frac{1}{1 + L_q d\frac{C_p}{2\sigma_{IF}^2}k_d}. \tag{37}$$

In the absence of quantization and pseudolite signal, the coherent output SNR is given by:

$$SNR_{out}^i = \frac{CN}{\sigma_{IF}^2}. \tag{38}$$

Thus, the loss caused by a pulsed pseudolite signal under the small signal approximation is given by

$$L_{ss} = L_q\frac{1}{1 + L_q d\frac{C_p}{2\sigma_{IF}^2}k_d} \tag{39}$$

that is given by the product of the quantization loss and the noise increase caused by the pseudolite signal. Under the hypothesis of ideal front-end filtering

$$\sigma_{IF}^2 = N_0 \frac{f_s}{2} \tag{40}$$

and

$$SNR_{out} = 2\frac{C}{N_0} T_c \cdot L_q \cdot \frac{1}{1 + L_q \frac{C_p}{N_0} d T_s k_d} \approx 2\frac{C}{N_0} T_c \cdot L_q \cdot \frac{1}{1 + L_q \frac{C_p}{N_0} d k_a} \tag{41}$$

where $k_a \approx T_s k_d$ is the analog SSC. It is noted that the impact of the pseudolite signal is reduce by the quantization loss and the duty cycle d. The use of a short duty cycle effectively reduces the transmitted power and thus the impact of the pseudolite signal.
It is noted that the term $\frac{C_p}{N_0}$ represents the peak pseudolite C/N_0. The adjective 'peak' is used to denote the fact that the $\frac{C_p}{N_0}$ does not account for the pulsing scheme that effectively reduces the transmitted (and received) power by a factor d. $\frac{C_p}{N_0}$ is computed by considering $y_p(t)$ alone as if the pseudolite signal were unpulsed. The effective C/N_0 of a pulsed pseudolite signal is defined as

$$\left.\frac{C_p}{N_0}\right|_{eff} = \frac{C_p}{N_0} d. \tag{42}$$

It is noted that for continuous pseudolite signals, $d = 1$ and $\left.\frac{C_p}{N_0}\right|_{eff} = \frac{C_p}{N_0}$. To ensure a fair comparison between pulsed and continuous pseudolite transmissions the C/N_0 of the two signals must be identical. This implies that the amplitude of the pulsed transmission must be a factor of $1/\sqrt{d}$ higher than the amplitude of the continuous transmission. Using the effective C/N_0, (41) can be rewritten as

$$SNR_{out} \approx 2\frac{C}{N_0} T_c \cdot L_q \cdot \frac{1}{1 + L_q \left.\frac{C_p}{N_0}\right|_{eff} k_a}. \tag{43}$$

3.2 Saturation Mode

Saturation is the condition where the input analog signal is so powerful that the ADC produces and output sequence assuming values in the set $\{\pm A_{\max}\}$ where A_{max} is the maximum value representable by the ADC. When considering saturation, it is assumed the pseudolite signal is so powerful to be always represented by the minimum and maximum values of the quantization function $Q_B(\cdot)$. Under saturation, it is not possible to use the results derived under the small signal assumption that is violated by the pseudolite signal.
In the case of a uniform quantizer

$$A_{max} = 2^B - 1. \tag{44}$$

Under saturation conditions, a convenient model for (13) is given by:

$$r_q[n] = Q_B(A_g(y_{IF}[n] + \eta_{IF}[n]))(1 - p[n]) + A_{max}\text{sign}\left(y_{p,IF}[n]\right) p[n] \tag{45}$$

In (45), the pseudolite signal, $y_{p,IF}[n]$, is always saturating the ADC and thus it assumes values equal to A_{max}. In addition to this, useful signal and noise components are effectively blanked by the pseudolite pulse justifying the presence of the $(1 - p[n])$ term in (45). Eq. (45) is used in the following to determine the loss caused by a pulsed pseudolite signal when the ADC is operating in saturation mode.

In order to compute the coherent output SNR, it is necessary to characterize the different terms present in P. In this case, it possible to decompose P as

$$P = P_q + P_I \tag{46}$$

where P_q is obtained by correlating the signal and noise term, $Q_B\left(A_g\left(y_{IF}[n]+\eta_{IF}[n]\right)\right)$, and P_l is determined by processing the pseudolite component $A_{max}\text{sign}\left(y_{p,IF}[n]\right)p[n]$. Using an approach similar to that adopted in Section 3.1, it is possible to show that under perfect frequency and delay alignment

$$E\left[P_q\right]=\sqrt{\frac{C}{2\sigma_{IF}^2}}a(1-d)\exp\left\{j\Delta\varphi\right\} \tag{47}$$

where $\Delta\varphi$ is the residual phase difference between local and incoming signals.
It is noted that the blanking performed by the pseudolite pulse reduces the signal amplitude by a factor equal to $(1-d)$ whereas the factor a models the effect of ADC/ADC [11]. Perfect frequency and delay alignment are the results of the maximization process performed in (15). In a similar way,

$$\text{Var}\left\{P_q\right\}=\frac{b}{N}(1-d). \tag{48}$$

P_l is obtained by correlating the term $A_{max}\text{sign}\left(y_{p,IF}[n]\right)p[n]$ with the locally generated code and carrier. The variance of P_l can be expressed in a similar way as is (27):

$$\text{Var}\left\{P_l\right\}=\frac{A_{max}^2}{N}\int_{-0.5}^{0.5}G_{pl}(f)G_c(f)df=\frac{A_{max}^2}{N}d\int_{-0.5}^{0.5}\bar{G}_{pl}(f)G_c(f)df=\frac{A_{max}^2}{N}dk_d \tag{49}$$

where $G_{pl}(f)$, $G_c(f)$ and $\bar{G}_{pl}(f)$ are as defined in Section 3.1. For the derivation of (49), it has been assumed that $c_p[n]$ is a bipolar sequence and $\text{sign}\left(c_p[n]\right)=c_p[n]$.
Thus, assuming independence between noise and pseudolite components, the coherent output SNR in the presence of pseudolite signal and with a saturating ADC becomes

$$SNR_{out}=\frac{NC}{\sigma_{IF}^2}\frac{a^2(1-d)^2}{b(1-d)+A_{max}^2dk_d}=\frac{NC}{\sigma_{IF}^2}\frac{L_q\cdot(1-d)}{1+k_dg(B,A_g)\frac{d}{1-d}} \tag{50}$$

where $g(B,A_g)$ defines the post-quantization Pseudolite-to-Noise Ratio (PNR) and models the effect of saturation on the pseudolite signal. When considering a uniform quantizer

$$g(B,A_g)=\frac{\left(2^B-1\right)^2}{1+8\sum_{i=0}^{2^{B-1}-1}i\text{erfc}\left(\frac{i}{\sqrt{2}A_g\sigma_{IF}}\right)} \tag{51}$$

and the loss due to quantization and pulsed interference becomes

$$L_{sat}=\frac{L_q\cdot(1-d)}{1+k_dg(B,A_g)\frac{d}{1-d}}=\frac{L_q\cdot(1-d)^2}{1-d+k_dg(B,A_g)d}. \tag{52}$$

Loss (52) clearly shows a quadratic dependence on the pulse duty cycle as in [13]. In addition to this, the SNR is degraded by three factors:

- **quantization**: a quantization loss, L_q, is introduced independently from the presence of pulsed interference
- **blanking**: the pseudolite pulse effectively blanks the useful signal and noise components leading to an SNR reduction equal to $(1-d)$
- **noise increase**: at the correlator output, the pseudolite pulse is perceived as an additional noise term that is proportional to the post-quantization PNR and the relative duration of the pulse $d/(1-d)$.

It is noted that (52) significantly differs from previous attempts to quantify the degradation introduced by pulsed pseudolite signals [2, 13] in the presence of saturation. Previous results where often provided without proof or neglecting the impact of the AGC/ADC.
Eq. (52) can be easily generalized to the case where several pulses arriving from different pseudolites

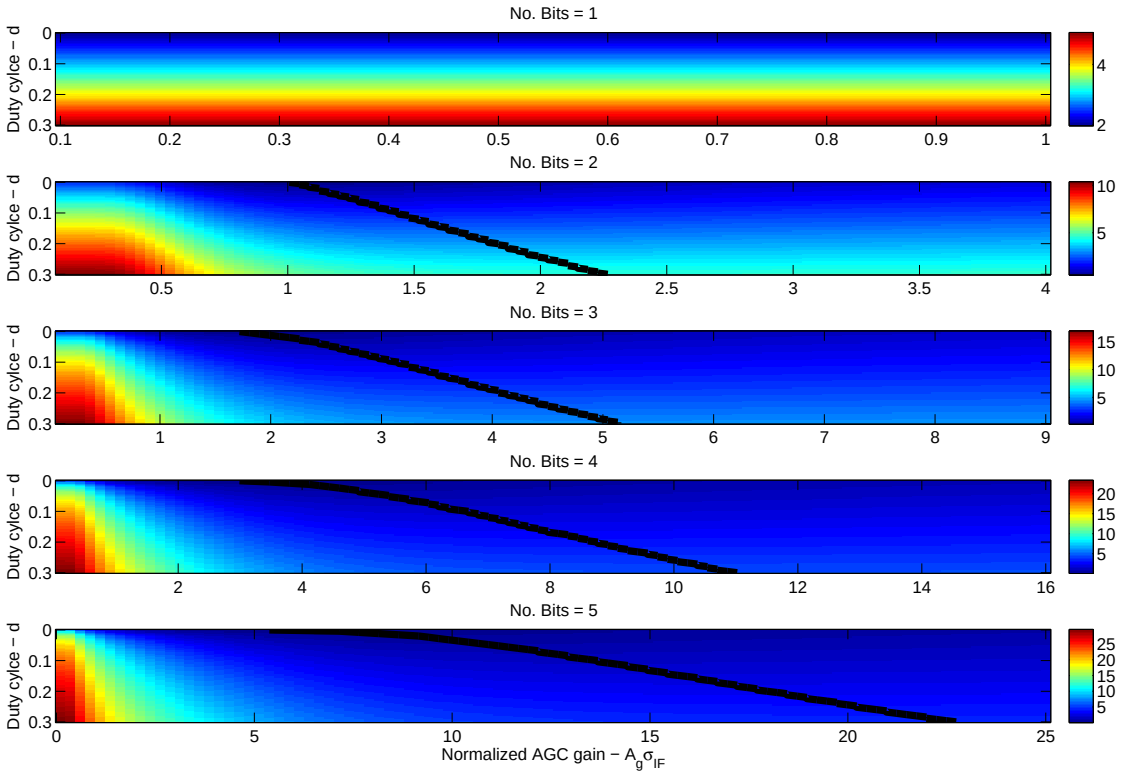

Figure 2: Loss in dB caused by a pulsed pseudolite signal as a function of the number of bits, pulse duty cycle and normalized AGC gain, $A_g\sigma_{IF}$. Dark thick lines in the plots indicate the optimal AGC gain that minimizes the loss for a given pulse duty cycle.

reach the non-participating receiver antenna. In this case, d is replaced by the percentage of time the receiver is blinded by the pseudolite pulses.
Loss (52) is analyzed in Fig. 2 where the loss caused by the pseudolite signal is shown as a function of the normalized AGC gain and the pulse duty cycle for different number of bits. In this case, it is assumed that the pseudolite Power Spectral Density (PSD) is flat within the receiver bandwidth and thus

$$\bar{G}_{pl}(f) = 1 \quad \text{for } -0.5 < f \leq 0.5 \tag{53}$$

$$k_d = \int_{-0.5}^{0.5} \bar{G}_{pl}(f) G_c(f) df = \int_{-0.5}^{0.5} G_c(f) df = 1. \tag{54}$$

This case represents for example the situation where the chipping rate of the pseudolite signal is higher than the receiver front-end bandwidth. The Radio Technical Commission for Aeronautics (RTCA) standard [13] considered a pseudolite standard based on the GPS Precision (P) code that has thus a chipping rate 10 times higher that that of the GPS L1 C/A code. This type of signal would lead to a $k \approx 1$ when recovered by a narrow band GPS L1 C/A receiver.
As expected, for $B = 1$ the loss is independent from the normalized AGC gain, $A_g\sigma_{IF}$. In multi-bit ADCs, the loss strongly depends on the AGC gain. Dark thick lines in Fig. 2 indicate the optimal AGC gain that minimizes the loss for a given pulse duty cycle. For a duty cycle of zero the optimal AGC gain is the usual value that minimizes the quantization loss [11]. As the duty cycle increases, the optimal AGC gain also increases, with two effects: increase of the quantization loss, L_q, and reduction of the PNR, $g(B, A_g)$. Thus, the optimal A_g is selected as a compromise between the quantization loss and the noise increase caused by the pulsed pseudolite signal. From Fig. 2, it is possible to note that, when the AGC gain is not properly set, multi-bit ADCs are more impacted by pseudolite signals. This phenomenon is essentially due to the fact that additional bits are available for the representation of the interfering signal.
The loss obtained when the ADC is operating in saturation mode is further inverstigated in Fig. 3 where Monte Carlo simulations have been used to support the theoretical results derived above. Simulations

Table 1: Simulation parameters adopted for determining the saturation loss introduced by a pulsed pseudolite signal.

Parameter	Value
Sampling Frequency, f_s	5 MHz
IF Frequency, f_{IF}	1.42 MHz
Integration Time, T_c	1 ms
No. of Simulation Runs	1e5
k_d	1

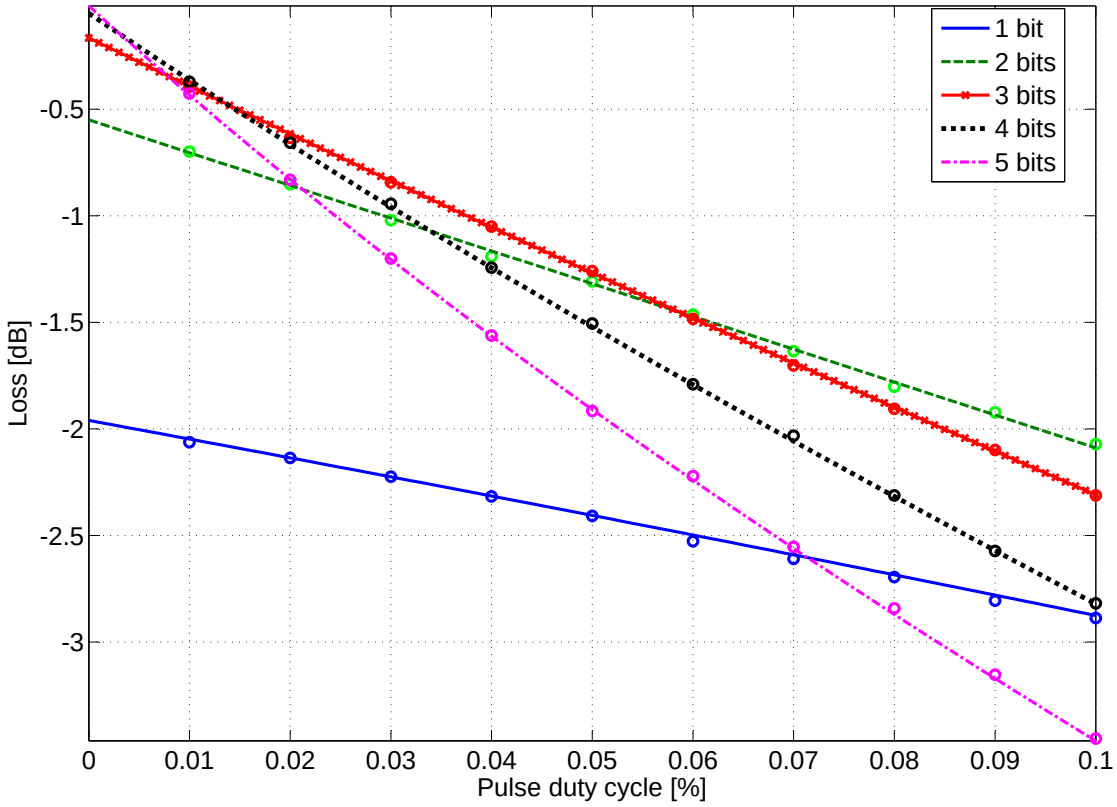

Figure 3: Loss caused by a pulsed pseudolite signal as a function of the number of bits and the pulse duty cycle. Comparison between theoretical and simulation results. Small circles represent simulation results.

were performed considering noisy GPS L1 C/A signals jammed by a pulsed pseudolite signal. The simulation parameters adopted for the evaluation of the saturation loss are reported in Table 1. In Fig. 3 the loss caused by a pulsed pseudolite signal is provided as a function of the number of bits and the pulse duty cycle. Small circles represent simulation results whereas lines have been obtained using (52). A good agreement between theoretical and simulation findings is observed supporting the validity of the proposed analytical model. In Fig. 3, the case of an ideal AGC has been considered and its gain has been fixed according to the formula

$$A_g = \frac{1}{\sigma_{IF}}\sqrt{3^{(B-2)}} \tag{55}$$

that effectively approximates the optimal AGC gain determined in [11]. When the pulse duty cycle tends to zero, the total loss tends to the quantization loss alone justifying the different intercepts with the y-axis. It is also noted that the curves in Fig. 3 have different slopes. This is due to the fact $g(B, A_g)$ increases with the number of bits when the (55) is valid. This is in agreement with the fact that multi-bit receivers are more sensitive to pulsed interference [2].

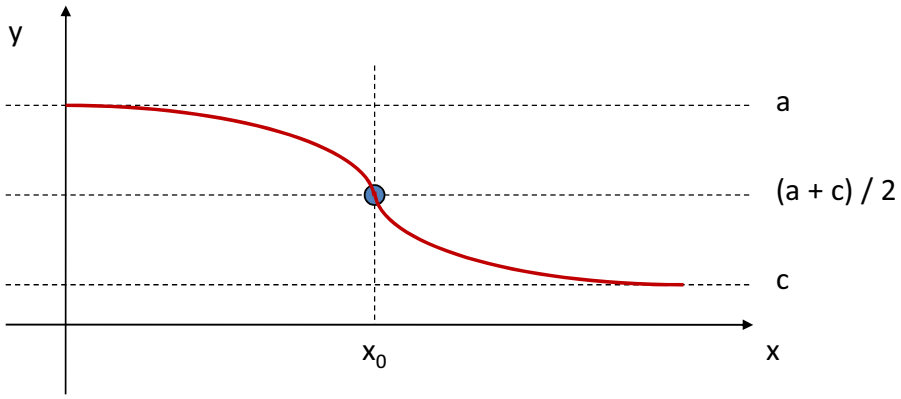

Figure 4: Schematic representation of the sigmoidal function adopted for interpolating the pseudolite loss.

3.3 Composite Loss Model

The small signal approximation and the loss obtained for saturating ADC can be combined to lead to the composite model

$$L_{pl} = \max\{L_{ss}, L_{sat}\} = L_q \cdot \max\left(\frac{1}{1 + L_q \frac{C_p}{N_0} dk_a}; \frac{1-d}{1 + k_d g(B, A_g) \frac{d}{1-d}}\right) \tag{56}$$

where L_{ss} is the loss determined in (39) and L_{sat} is the loss (52) determined when the ADC operated in saturation mode. In (56), the loss computed when the receiver operates in saturation mode lower bounds the loss computed obtained using the small signal approximation. It is noted that the loss caused by a pseudolite signal is bounded by the quantization and saturation losses. Quantization loss is an upper bound whereas the saturation loss represents a lower limit of the degradation caused by the pseudolite signal. When continuous pseudolite signals are considered then L_{sat} = 0 (d = 1) and L_{pl} (expressed in dB units) grows without bounds.

Although model (56) is an useful tool for predicting the loss caused by a pseudolite signal, poor prediction performance can be obtained when operating in the region at the interface between small signal and saturation regimes. Model (56) can thus be further improved by better modeling the transition between the two mentioned conditions. Finding a solution directly incorporating these two regimes as special cases is a difficult task that does not seem to admit a simple closed-form solution. This problem is overcome here by adopting an interpolation function that guarantees a smooth transition between small signal and saturation conditions.
The fact that the pseudolite loss is always bounded from above and below suggests the use of a sigmoidal function that is characterized by two horizontal asymptotes. More specifically, a sigmoidal function can be defined as

$$y(x) = a + \frac{c-a}{1 + \exp\{-(b(x - x_0)\}} \tag{57}$$

where

- a and c are two constants defining the horizontal asymptotes of $y(x)$;
- b controls the transition speed between a and c;
- x_0 is a location parameter controlling the horizontal shift of the function.

The properties of the sigmoidal function adopted for interpolating the pseudolite loss are shown in Fig. 4. From Fig. 4, the following properties emerge:

$$a = \lim_{x \to -\infty} y(x) \tag{58}$$

$$c = \lim_{x \to +\infty} y(x) \tag{59}$$

$$y(x_0) = \frac{c+a}{2}. \tag{60}$$

Eqs. (58)-(60) provide a simples way to set the parameters of $y(x)$. b can be determined by considering the derivative of $y(x)$ computed at x_0:

$$\left.\frac{dy(x)}{dx}\right|_{x=x_0} = \left.\frac{b(c-a)\exp\{-b(x-x_0)\}}{(1+\exp\{-b(x-x_0)\})}\right|_{x=x_0} = b\frac{c-a}{4}. \tag{61}$$

From (61), it follows:

$$b = \frac{4}{c-a}\left.\frac{dy(x)}{dx}\right|_{x=x_0}. \tag{62}$$

This equation, along with (58), (59) and (60), allows one to determine all the parameters of the sigmoidal function (57). Even if the previous equations do not define an optimal procedure for fitting experimental data, they provide a simple way to determine the parameters of the sigmoidal function (57). For its simplicity this procedure procedure is thus preferred to more complex numerical approaches that for example minimize the Mean Square Error (MSE) between empirical and fitted data.
Sigmoidal interpolation is used to express the pseudolite loss as a function of the effective pseudolite C_p/N_0. Both effective C_p/N_0 and pseudolite loss are expressed in dB units and

$$L_{pl}|_{dB} = a + \frac{c-a}{1+\exp\left\{-(b\left(\left.\frac{C_p}{N_0}\right|_{eff,dB-Hz} - x_0\right)\right\}}. \tag{63}$$

The choice of applying sigmoidal interpolation in the double logarithmic domain is justified by the fact that $\left.\frac{C_p}{N_0}\right|_{eff}$ expressed in linear units is always positive. Thus, if interpolation were applied considering linear units, than the asymptote defined by a would never be reached.
Using the previous results, it is possible to show that

$$a = L_q|_{dB} \tag{64}$$

$$c = L_{sat}|_{dB} = 10\log_{10}\left(\frac{1-d}{1+k_d g(B,A_g)\frac{d}{1-d}}\right) \tag{65}$$

$$x_0 = \frac{\frac{1}{\sqrt{L_{sat}L_q}} - 1}{L_q k_a} = \frac{10^{-\left(L_{sat}|_{dB} + L_q|_{dB}\right)/20} - 1}{10^{L_q|_{dB}/10} k_a} \tag{66}$$

$$b = -\frac{4}{L_{sat}|_{dB} - L_q|_{dB}}\frac{k_a 10^{x_0/10}}{1+k_a 10^{x_0/10}}. \tag{67}$$

Eqs. (66) and (67) have been obtained by assuming that for a loss equal to $\frac{L_{sat}|_{dB} + L_q|_{dB}}{2}$, the receiver is still operating in the small signal regime.
It is noted that using the properties of the sigmoidal function (57) it is possible to completely specify the loss model as a function of only three parameters:

- the saturation loss
- the quantization loss
- the analog SSC.

This allows a simple analytical treatment of the loss introduced by pseudolite signals. It is noted that when multi-bits receivers are employed the quantization loss can be neglected and $L_q = 1$ ($L_q|_{dB} = 0$). In the following sections, the quantization loss will be neglected.

In order to determine the accuracy of approximations (56) and (63) several Monte Carlo simulations have been run as a function of the effective pseudolite C/N_0. The same parameters used for the evaluation of the saturation loss and reported in Table 1 have been used for the analysis.
Sample simulation results are reported in Figs. 5, 6, 7 and 8. Simulations have been performed by assuming a constant AGC gain. More specifically, A_g was set according to (55). The assumption of a constant AGC gain can be considered realistic for small duty cycles since short pulses are expected to have a small impact on AGC logic for the threshold setting. The proposed composite model provides a close approximation of the loss caused by a pulsed pseudolite signal.

From Figs. 5, 6, 7 and 8 it is possible to note that for low pseudolite C/N_0 values, the small signal approximation is actually an upper bound for the experienced loss. Quantization effects and violations of the assumptions made to derive (39) make the actual loss worse than the one theoretically predicted. Differences are however marginal. As the pseudolite signal power increases, saturation effects start appearing and the loss theoretically predicted becomes worse than the actual one. For high pseudolite effective C/N_0 values the loss estimated by simulation converges to the theoretical saturation loss that represents the worse case scenario.

Eqs. (56) and (63) will be used in Section 5 to determine critical parameters such as the minimum separation distance, maximum pseudolite transmitted power and maximum duty cycle corresponding to a predefined loss. In order to determine the minimum separation distance between pseudolites and non-participating GNSS receivers, it is necessary to express the pseudolite received power, C_p, in (56) as a function of the transmitted power and the transmitter-receiver distance. In the following, the free-space loss model is adopted and C_p is expressed as

$$C_p = P_{TX} \frac{G_{RX} G_{TX}}{L} \left(\frac{\lambda}{2\pi R} \right)^2 \tag{68}$$

where

- P_{TX} is the transmitted power
- G_{RX} and G_{TX} are the receiver and transmitter antenna gains
- L is the excess propagation loss (in this report, $L = 1$ will be assumed)
- λ is the wavelength of the pseudolite signal
- R is the distance between transmitter and receiver.

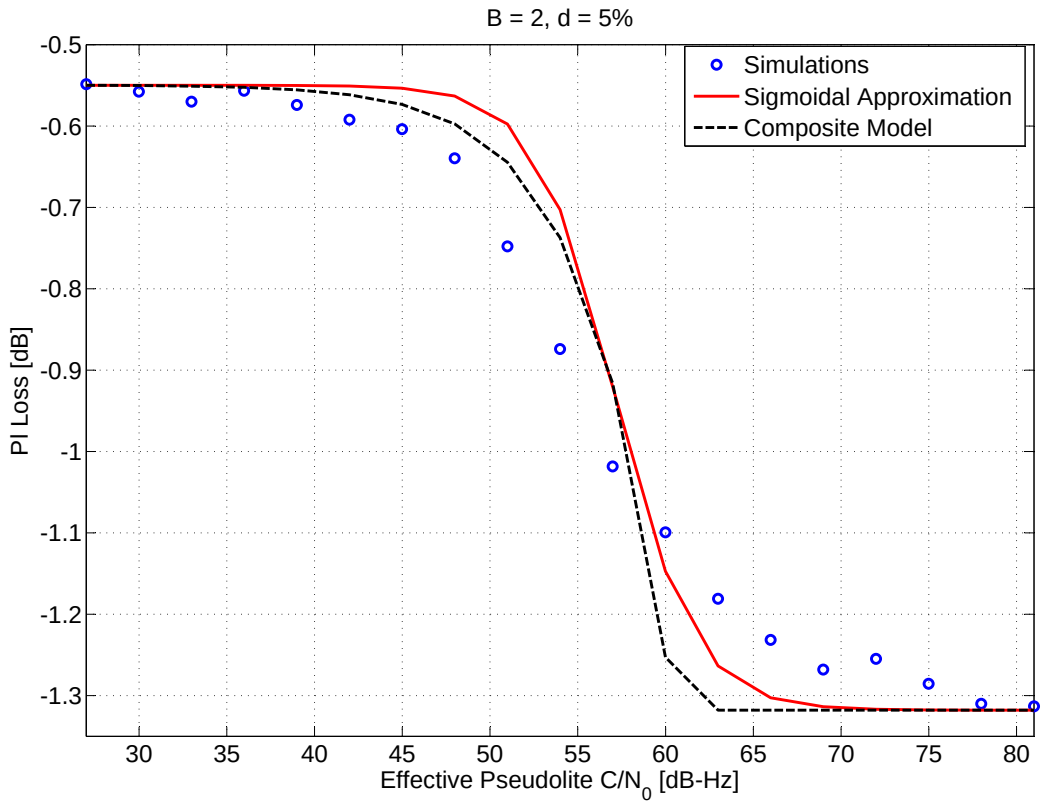

Figure 5: Loss caused by a pseudolite pulsed signal as a function of the effective pseudolite C/N_0. Comparison between Monte Carlo simulation and theoretical results. $B = 2$ and $d = 0.05$.

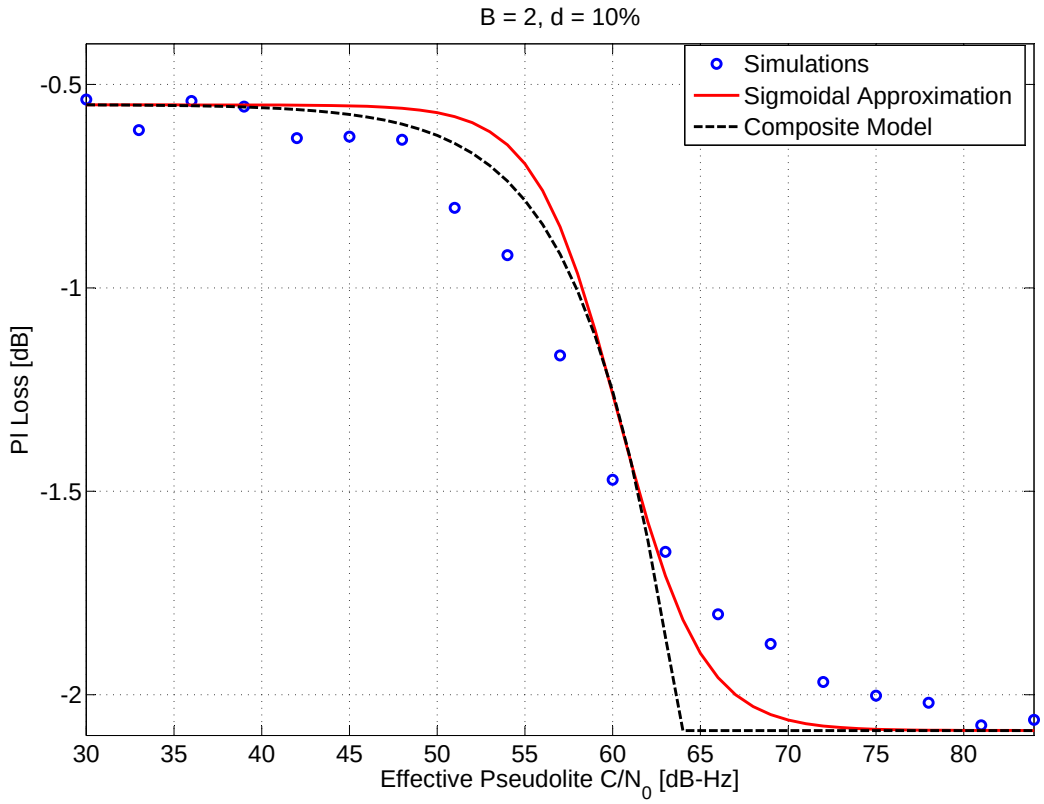

Figure 6: Loss caused by a pseudolite pulsed signal as a function of the effective pseudolite C/N_0. Comparison between Monte Carlo simulation and theoretical results. $B = 2$ and $d = 0.10$.

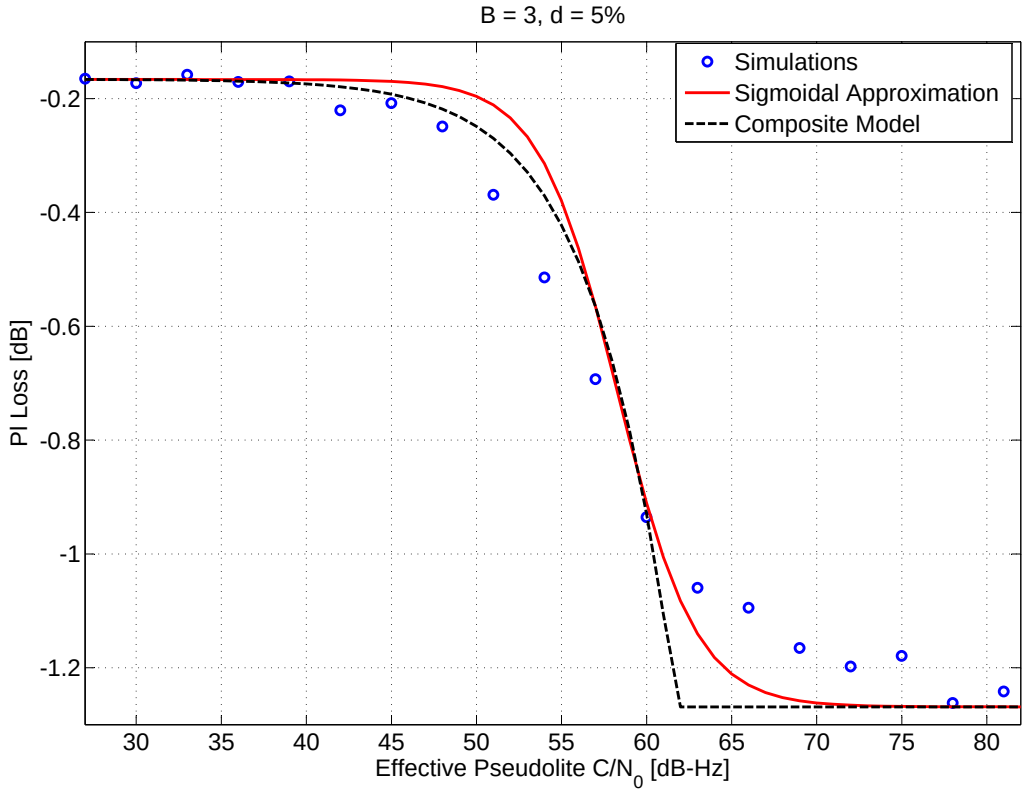

Figure 7: Loss caused by a pseudolite pulsed signal as a function of the effective pseudolite C/N_0. Comparison between Monte Carlo simulation and theoretical results. $B = 3$ and $d = 0.05$.

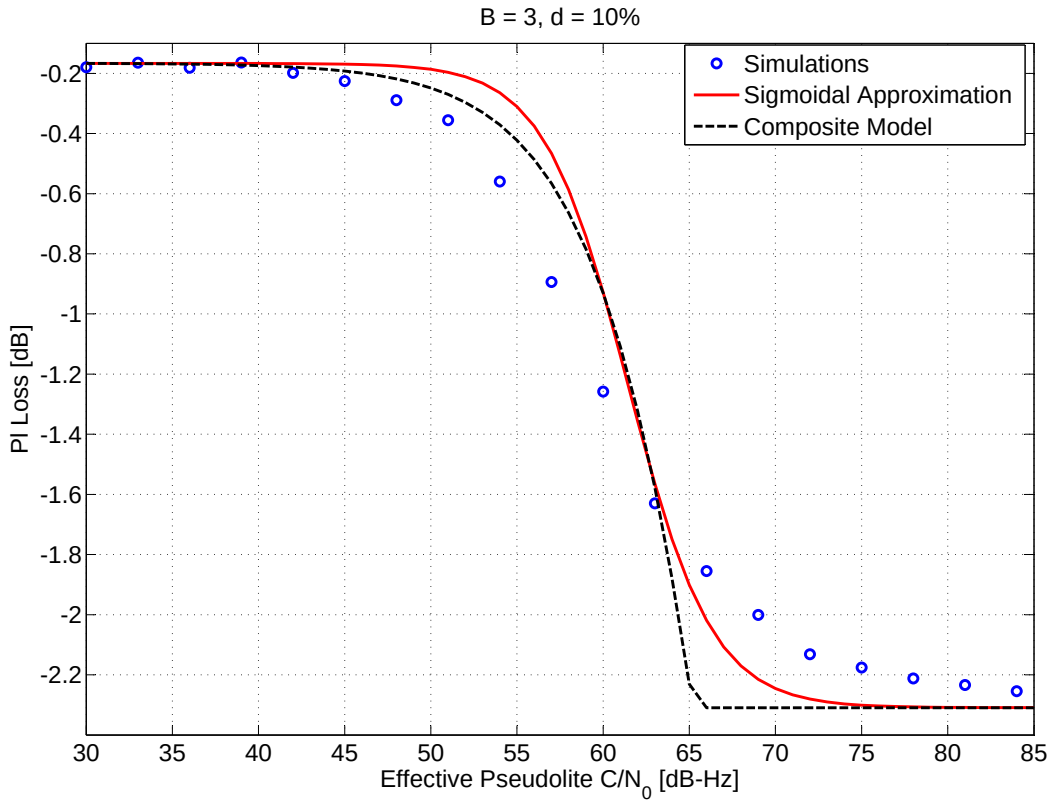

Figure 8: Loss caused by a pseudolite pulsed signal as a function of the effective pseudolite C/N_0. Comparison between Monte Carlo simulation and theoretical results. $B = 3$ and $d = 0.10$.

4 Experimental Setup and Analysis

In order to support the validity of the theoretical model derived in Section 3, several tests have been conducted using pseudolites and commercial GNSS receivers. Experiments have been performed both in conducted and radiated mode. In the conducted mode experiments, the output of a signal generator capable of generating GNSS as well as pseudolite signals was directly connected to the antenna port of the commercial GNSS receiver under test. A detailed description of the experimental setup adopted for experiments performed in conducted mode can be found in [5].
Radiated experiments were conducted in the anechoic chamber of the using up to three pseudolites. GPS L1 C/A and Galileo composite binary offset carrier (CBOC)(6, 1, 1/11) were generated using a Spirent GSS8000 simulator and broadcast inside the anechoic chamber along with the pseudolite signals. The Spirent GSS8000 is able to simultaneously simulate up to 16 GNSS signals, 8 GPS and 8 Galileo, and was used to determine the impact of pseudolite signals on both GPS and Galileo receivers. Pseudolite signals were generated using devices provided by SSF. The pseudolites from SSF are able to produce both continuous and pulsed signals with selectable duty cycle and signal power. Views of the experimental setup used for the radiated experiments are shown in Figs. 9 and 10. The Spirent GSS8000 simulator was used to generate a scenario consisting of 8 GPS and 8 Galileo satellites having a constant power. The signal power was set such that the receiver under test estimated, in the absence of pseudolite signals, a C/N_0 of about 43 dB-Hz. All the satellite signals have the same power.
The loss induced by the pseudolite signal has been evaluated as the difference between C/N_0 values estimated in the presence and absence of pseudolite interference:

$$L|_{dB} = \left.\frac{C}{N_0}\right|_{\text{with pl},dB} - \left.\frac{C}{N_0}\right|_{\text{no pl},dB} \tag{69}$$

where the subscripts “no pl”, “with pl” indicate the absence and presence of pseudolite signal, respectively. The C/N_0 in the absence of pseudolite signal was obtained in the baseline test conducted with GNSS signals only.
It is noted that this approach does not allow one to measure the quantization term in (52) and (39). The quantization loss is not observable since the signal at the input of the receiver is quantized independently from the pseudolite component.
In the following experimental results obtained for the cases detailed in Table 2 are reported. Two experiments are considered in this report:

1. Constant duty cycle: the pseudolite power level is progressively increased to observe the onset of saturation

2. Constant power: the duty cycle is progressively increased in order to extract the effective pseudolite SNR at saturation.

Both experiments consist of a single pseudolite

In all experiments the pseudolite was configured to transmit the GPS C/A code for PRN number 2, since this PRN was not present in the simulation data set. Thus, the receivers under test were able to track the pseudolite signal, thereby yielding a measure of the pseudolite C/N_0. Note that the receivers were not configured to apply any pulsing blanking and therefore the pseudolite C/N_0 as measured by the receivers is given by:

$$\left.\frac{C_p}{N_0}\right|_{\text{meas}} = d^2 \left.\frac{C_p}{N_0}\right|_{\text{peak}} = d \left.\frac{C_p}{N_0}\right|_{\text{eff}}.$$

Table 2: Receivers and signals considered for the compatibility analysis.

Receiver Model	Signal
u-Blox 5	BPSK(1) GPS L1 C/A
Javad	BPSK(1) GPS L1 C/A
Javad	CBOC(6,1,1/11) Galileo E1

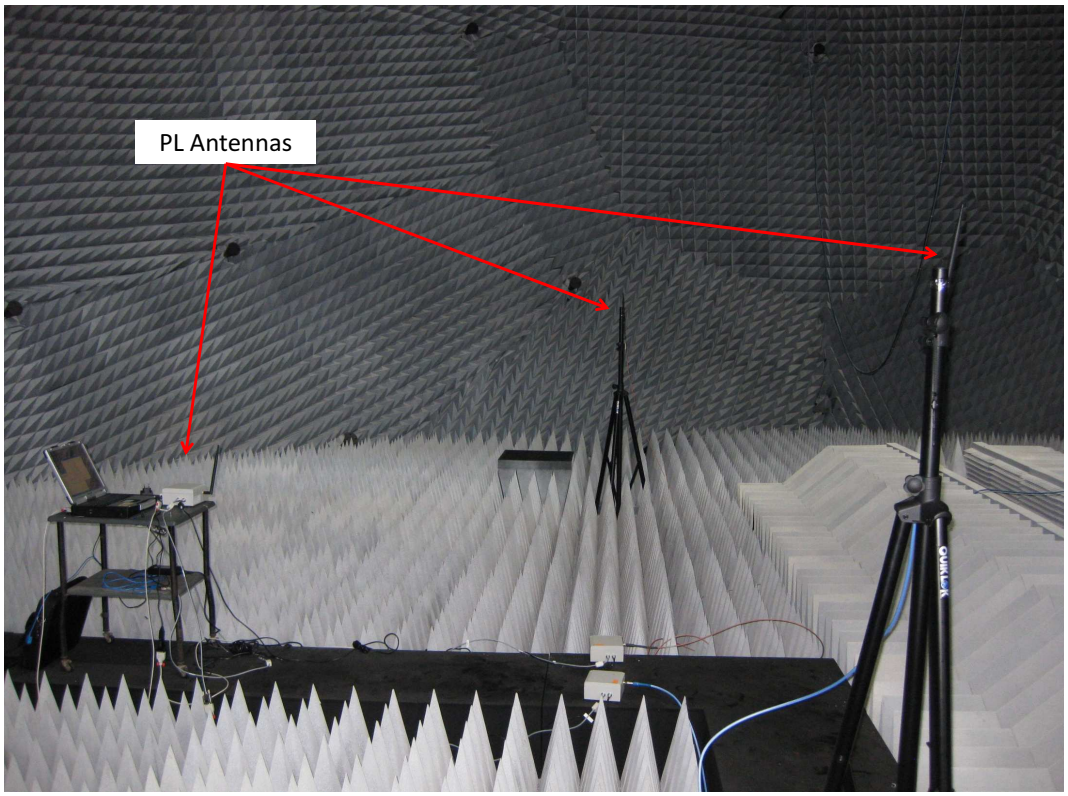

Figure 9: Location of the three pseudolites used for the radiated tests. Tests were performed inside an anechoic chamber and the pseudolite were placed about 5 meters form the receiver antenna.

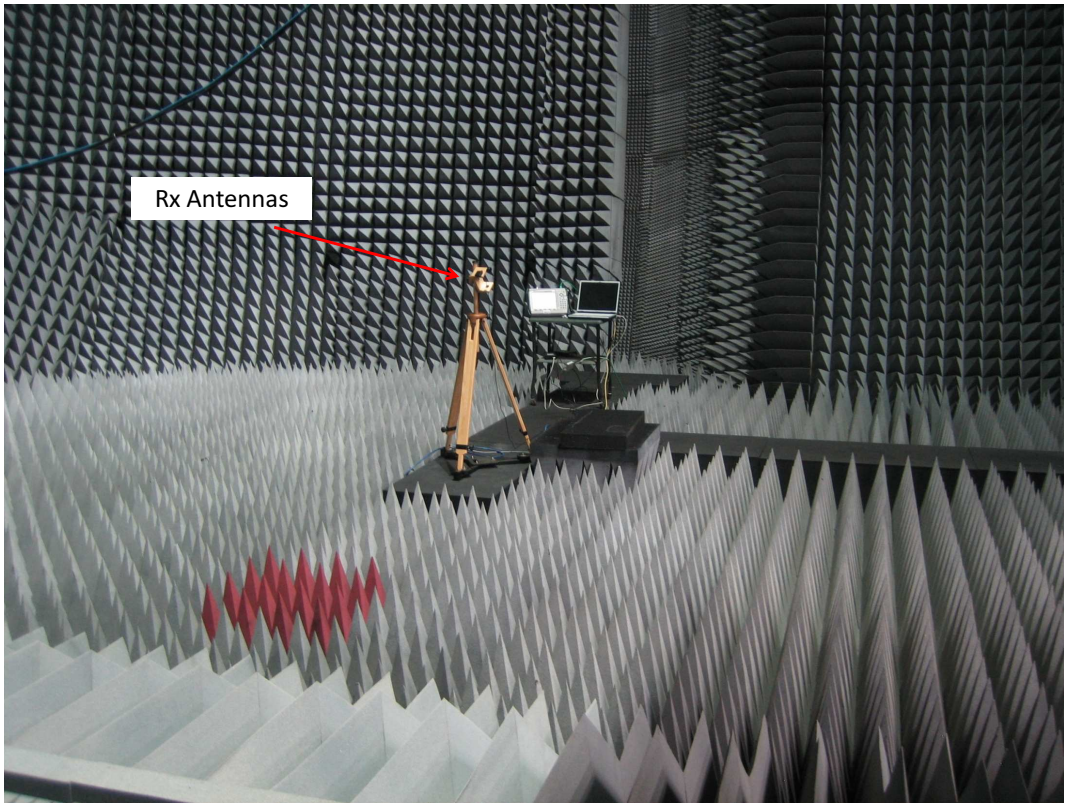

Figure 10: Location of the GNSS receiver antenna used for the radiated tests.

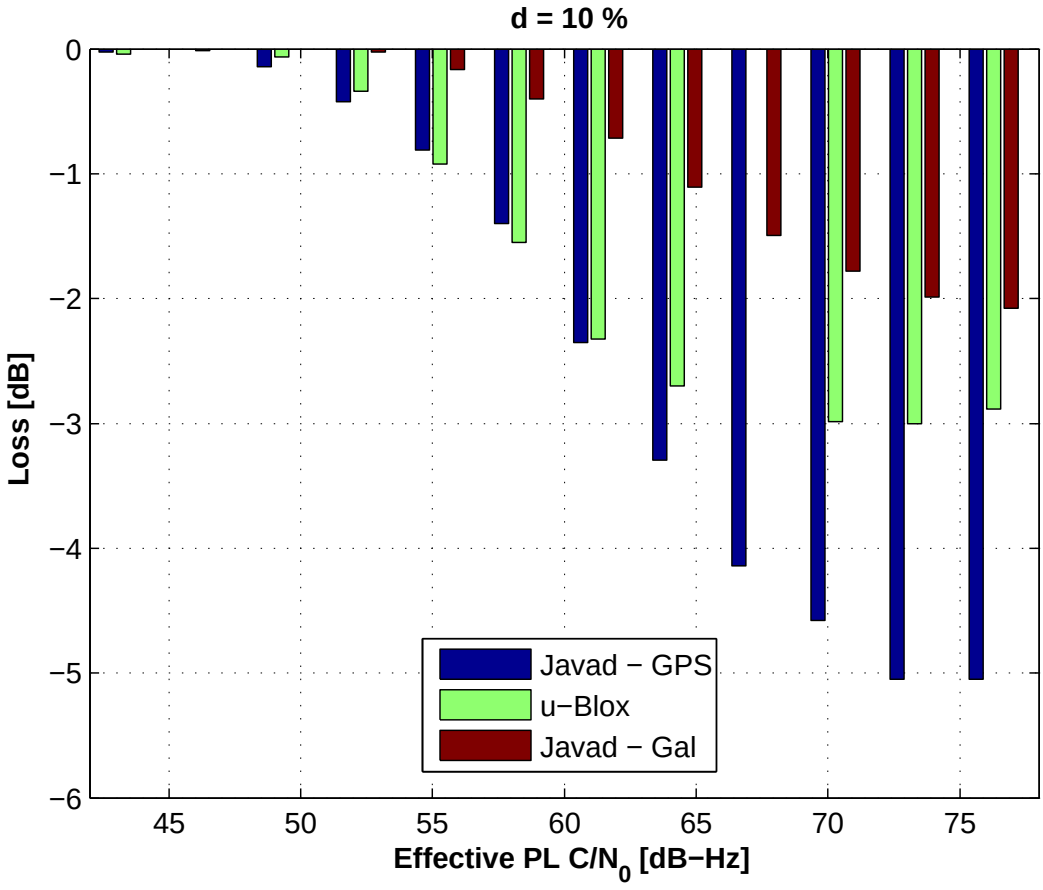

Figure 11: Measured pseudolite loss as a function of the effective pseudolite power. Constant duty cycle, d = 10%.

4.1 Constant duty cycle experiments

The first set of experiments involved a single pseudolite with a 10% duty cycle. The power level of the pseudolite was initially configured such that the receiver experienced an effective C/N_0 of $\sim$ 43 dB-Hz. The power level was held constant for a period of five minutes and then increased by 3 dB every 5 minutes up to a maximum pseudolite C/N_0 of $\sim$ 76 dB-Hz. The average C/N_0 loss for each satellite in each 5 min period was computed by comparing the measured C/N_0 with a baseline test conducted with no pseudolites. Histograms of the results are shown in Fig. 11.

The impact of the pulsing is clearly visible in the figure, with all three receiver types approaching saturation as the effective C/N_0 approaches 70 dB-Hz. It is also interesting to note that the high-precision (Javad) receiver suffers greater losses than the high sensitivity (u-Blox) receiver, due to its higher front-end bandwidth, and possibly greater bit resolution. Also, note that for the same receiver type, the impact of the (GPS) pseudolite on Galileo signals is significantly reduced compared to its impact on other GPS signals. This is due to the impact of the SSC as shown in (56). A comparison of the measured loss with that predicted by the small signal model of (43) is given in Fig. 12, where excellent agreement between theory and experiment can be seen. Note that the receivers are black boxes, the front-end bandwidth, bit resolution and AGC algorithm used are unknown and therefore the saturation model cannot be predicted. Hence only the small signal model is illustrated in the figure. Also, since the bit resolution is unknown, the quantization loss of (43) has been ignored.

The sigmoidal approximation of Section 3 can also be verified using this data. The results of fitting the experimental to the sigmoidal curve (ignoring the quantization loss) are shown in Fig. 13.

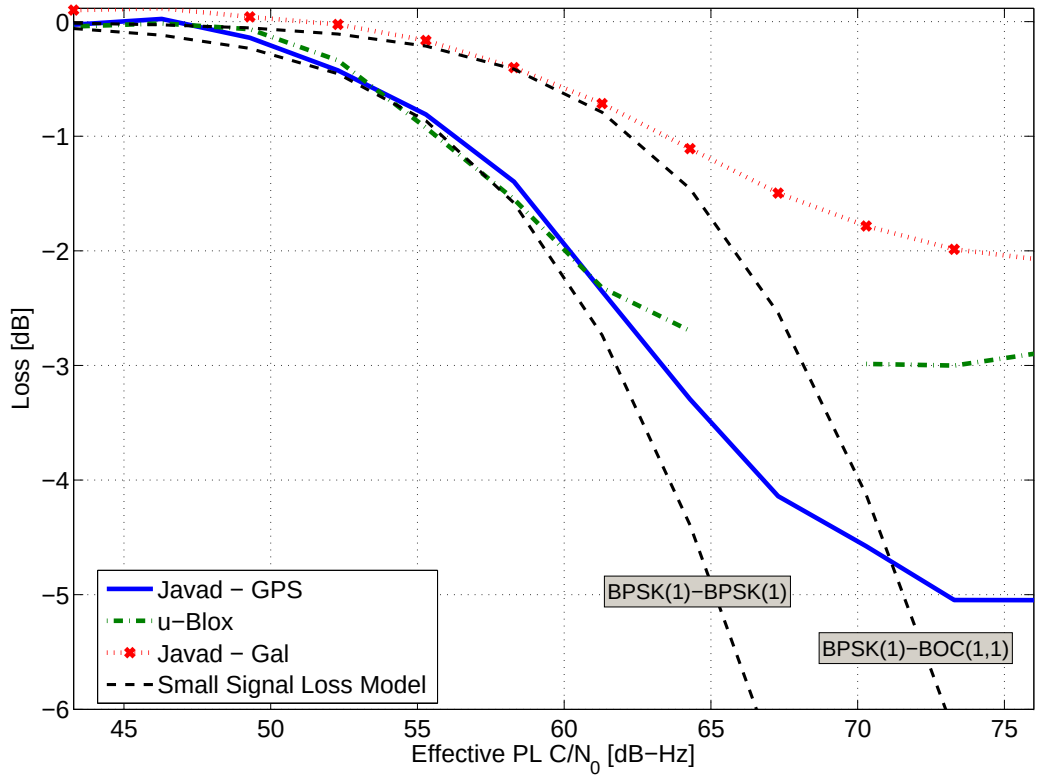

Figure 12: Comparison of the measured pseudolite loss against the small signal approximation model. For low pseudolite effective C/N_0 the loss closely follows the theoretical model independently from the receiver types. The SSC has been obtained from [1]. d = 10%.

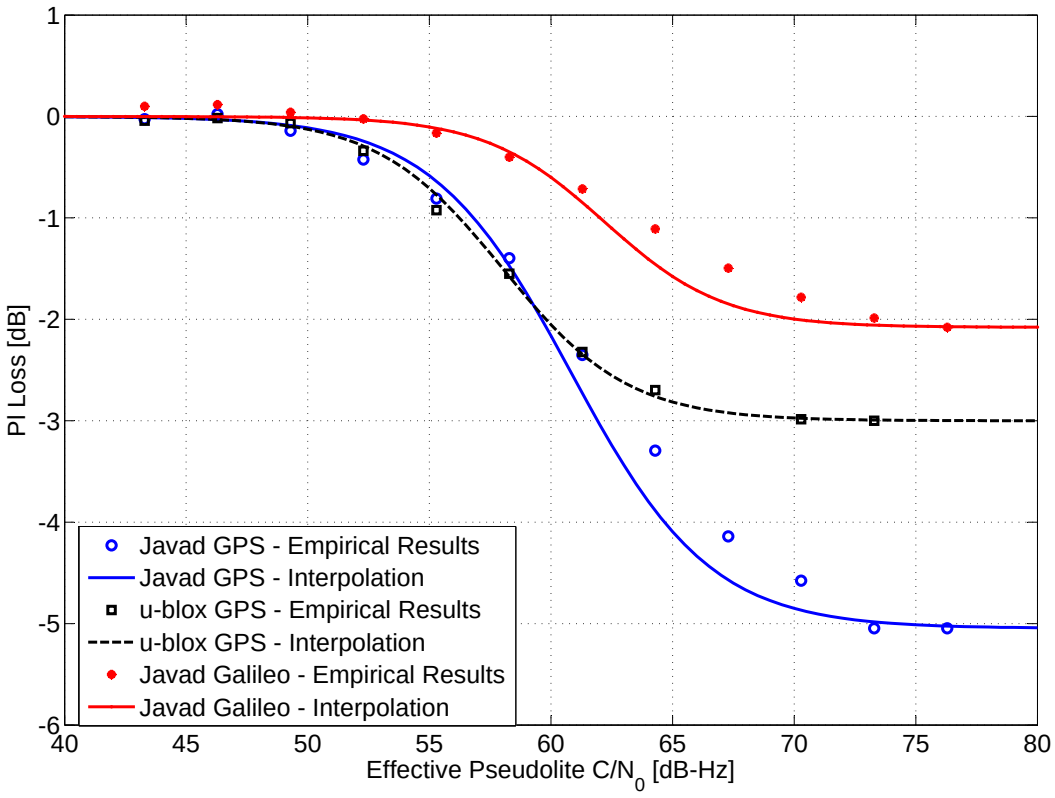

Figure 13: Pseudolite SNR loss vs effective C/N_0, experimental data and sigmoidal fit.

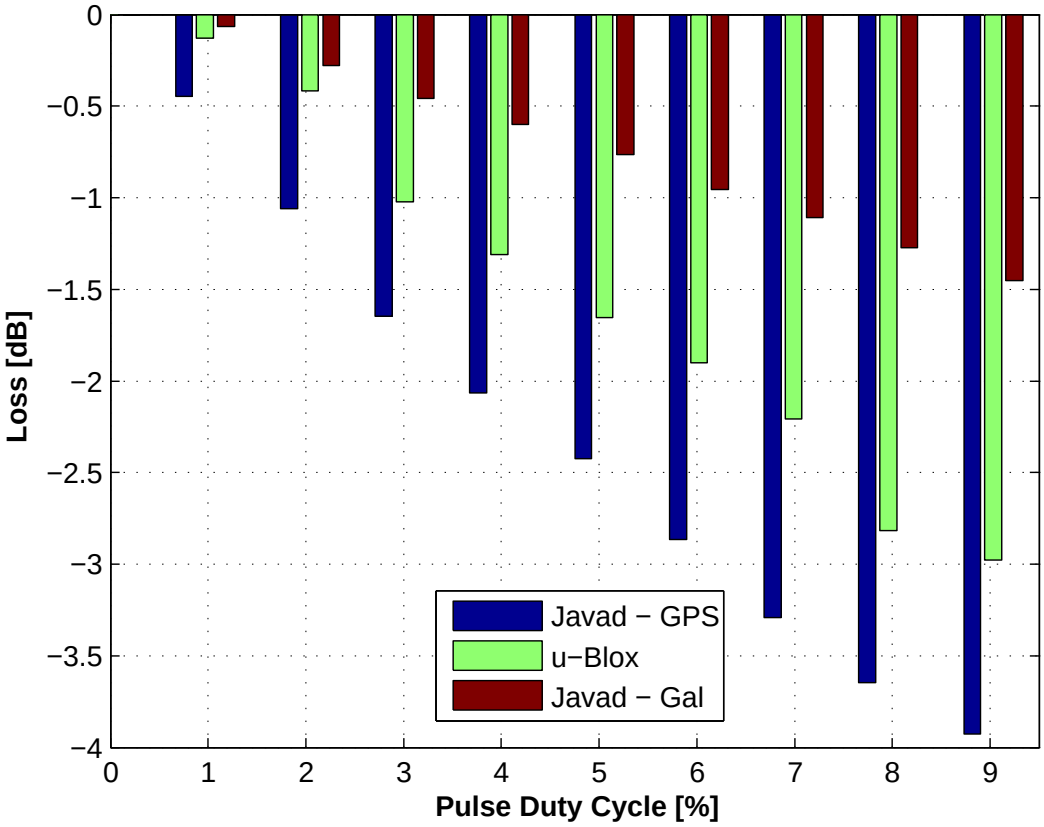

Figure 14: Measured saturation loss as a function of the pulse duty cycle.

4.2 Constant power experiments

For the second set of radiated mode experiments the pseudolite was configured to transmit such that the received power level induced saturation in both receivers. Following a similar approach as with the fixed duty cycle experiment, the duty cycle was initially set to approximately 1%, then increased by 1% in five minute intervals up to a maximum duty cycle of 9%. The average loss over each five minute interval was computed and the resulting histogram is shown in Fig. 14. The impact of increasing the duty cycle is clearly seen in the figure, with the saturation loss increasing monotonically with the duty cycle.

As discussed in the previous section, the receivers used can be considered as black boxes. However, the data extracted in Fig. 14 can be used to determine some receiver dependent parameters. From (52), it can be seen that the saturation loss can be re-written as;

$$L_{sat} = L_q \frac{(1-d)}{1 + \mathrm{SNR}_{\mathrm{sat}} \frac{d}{1-d}},$$

where

$$\mathrm{SNR}_{\mathrm{sat}} = k_d g(B, A_g), \tag{70}$$

is the pseudolite-induced *saturation SNR*, that is the SNR of the pseudolite signal at the correlator output when the receiver is saturated. This term is a function of the receiver front-end bandwidth, bit resolution and AGC algorithm, but should be independent of the pulse duty cycle. Fig. 15 shows the $\mathrm{SNR}_{\mathrm{sat}}$ values computed from the data in Fig. 14.

The near constancy of the estimate value of $\mathrm{SNR}_{\mathrm{sat}}$ suggests that the saturation model is accurate. For low values of the duty cycle (around 1%) it can be seen that the $\mathrm{SNR}_{\mathrm{sat}}$ value is not well estimated. This is due to the fact that the losses are so small in this region and the C/N_0 measurement noise dominates the estimation process. While the lack of knowledge of the receiver parameters implies that $\mathrm{SNR}_{\mathrm{sat}}$ cannot be computed *a priori*, (70) suggests that it should be possible to predict, for example, the

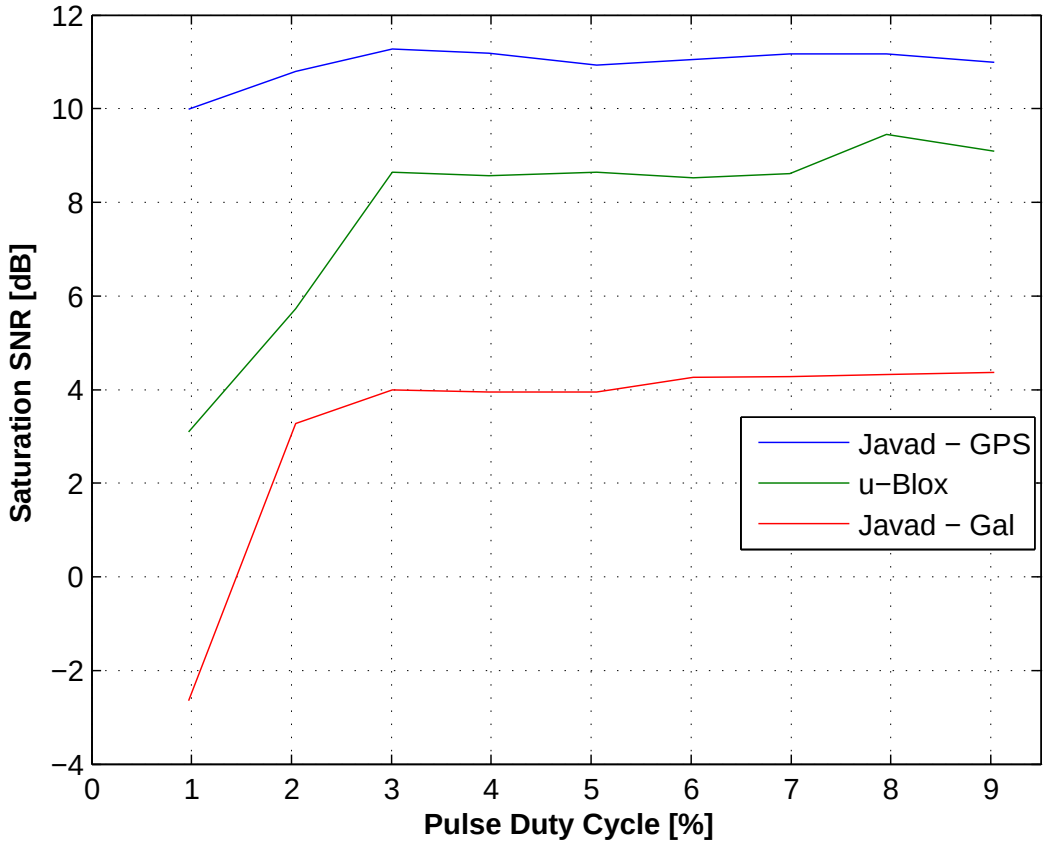

Figure 15: SNR_{sat} vs pulse duty cycle computed from experimental data

Table 3: Average SNR_{sat} values extracted from the data

Receiver	SNR_{sat} (dB)
u-Blox (GPS)	8.5
Javad (GPS)	11.1
Javad (Gal.)	4.1

loss experienced by a CBOC signal *given* the loss experienced by a BPSK signal:

$$SNR_{sat}|_{CBOC} = \frac{k_{d,CBOC}}{k_{d,BPSK}} SNR_{sat}|_{BPSK} .$$

Fig. 16 shows the measured Galileo SNR_{sat} and that estimated using the measured GPS value and the ratio of the GPS and Galileo SSCs vs pulse duty cycle. Here two values for the SSCs have been used: 1) the Galileo signal is modelled as BOC(1,1); 2) the Galileo signal is modelled as CBOC(6,1,1/11). There is close agreement between theory and measurement, though the match is not perfect. Differences may arise due to, for example, the impact of the receiver front-end on the SSC and the distortion of the pseudolite signal spectrum due to clipping. Table 3 records the mean values of SNR_{sat} extracted from the results shown in Fig. 15 ignoring the first two data points. This short table clearly shows the impact of the SSC and receiver front-end bandwidth on the effect of pseudolite signals on non-participating receivers. The average SNR_{sat} values recorded in Table 3 will be used in Section 5 to predict the behaviour of non-participating receivers in a number of case-studies.

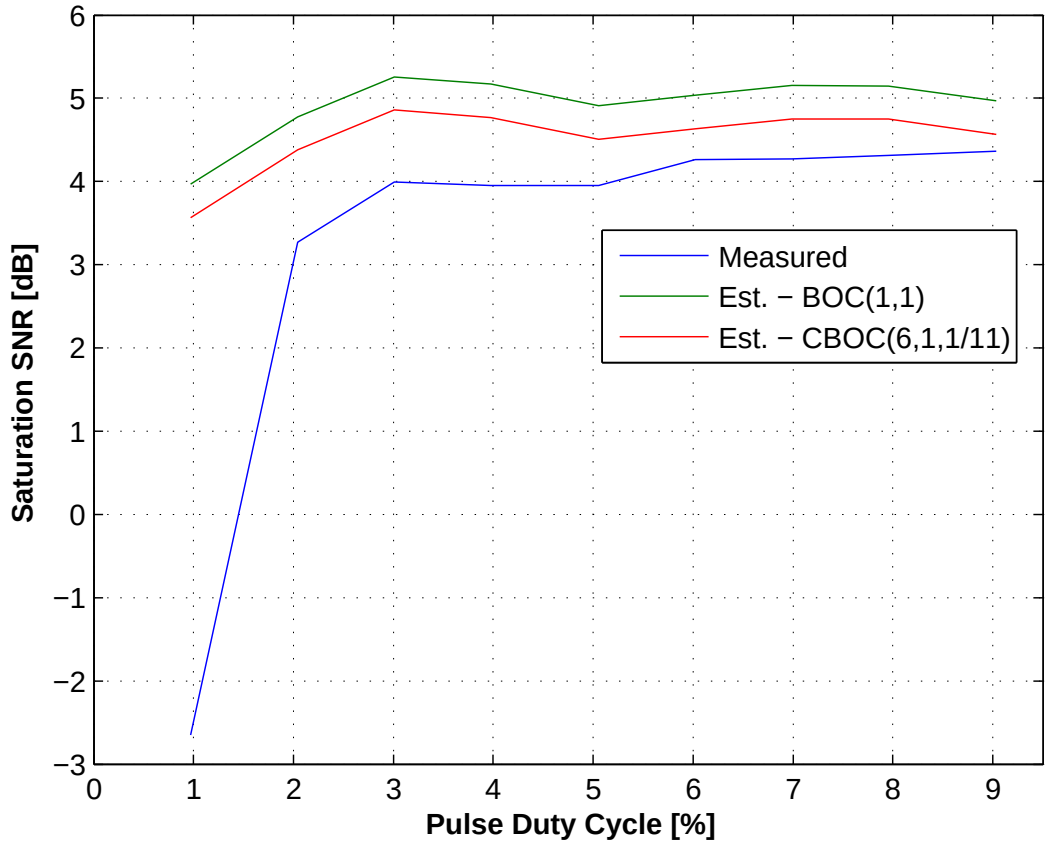

Figure 16: Measured and estimated $\mathrm{SNR}_{\mathrm{sat}}$ values for Galileo signals vs pulse duty cycle. Two values of the Galileo E1 SSC have been used: 1) BOC(1,1) vs BPSK SSC; 2) CBOC(6,1,1/11) vs BPSK SSC

5 Case Studies

In this section the experimental results from the previous section are used in conjunction with a number of sample pseudolite transmit power levels to determine the impact of pulsing. The following power levels have been recommended in two separate reports from the Electronic Communications Commission (ECC) of CEPT [4, 14]:

- -50 dBm
- -59 dBm
- -70 dBm.

Given the importance of the effective pseudolite C/N_0, as defined in (42), in this section we assume that the peak transmit power is adjusted as a function of the duty cycle, such that the *effective transmit power* is given by one of the above three values. In keeping with (42) the effective transmit power is defined as:

$$P_{Tx}|_{\mathrm{eff}} = P_{Tx}|_{\mathrm{peak}}\, d. \tag{71}$$

The minimum distance from the pseudolite required to keep the SNR loss below a certain threshold is chosen as a figure of merit:

$$R_{\mathrm{min}}\,(L_{\mathrm{th}}) = \arg\underset{R}{\,} L_{pl}(R) = L_{\mathrm{th}}, \tag{72}$$

where the relationship between R and the received pseudolite signal power C_p is given by (68). For example, choosing a 1 dB SNR loss threshold, the figure of merit is the minimum distance that a receiver must remain from the pseudolite to ensure that the average SNR loss is no greater than 1 dB. In the following, the three receiver configurations used in the experimental setup of the previous section are used to determine the appropriate minimum distances for the three transmit power levels given above and for two target SNR loss thresholds: 1) 1 dB; 2) 3 dB.

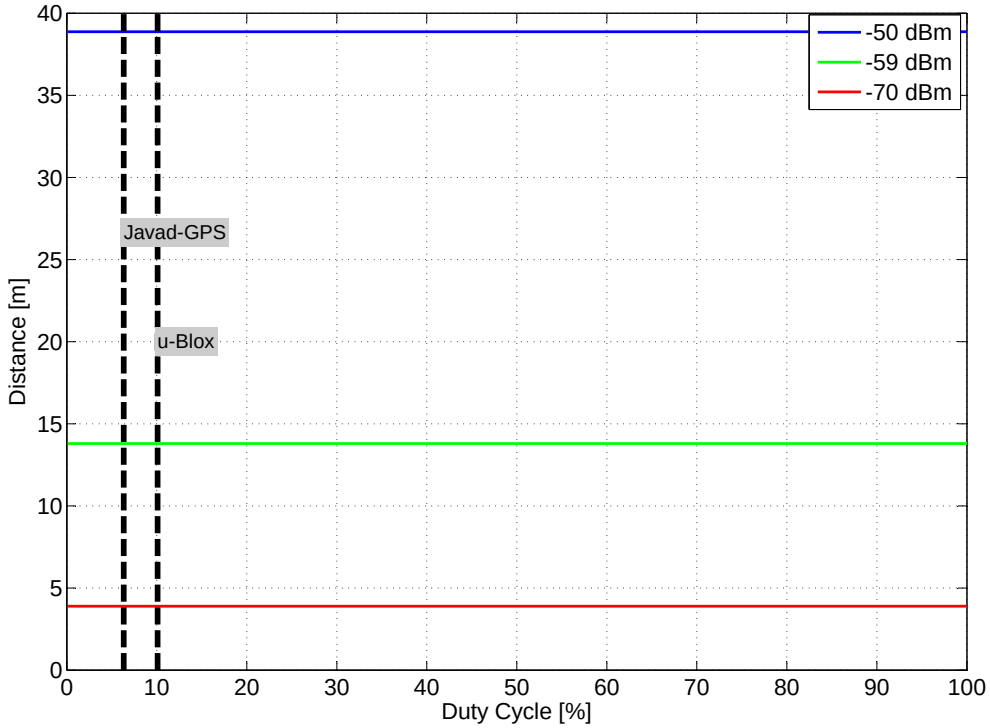

Figure 17: Minimum distance vs duty cycle for GPS C/A code signals under the small signal approximation. SNR loss threshold = 3 dB. The minimum duty cycles for the Javad and u-Blox receivers for which an SNR loss of 3 dB is possible are indicated with black dashed lines.

5.1 3 dB SNR Loss Threshold

In this section a maximum allowable SNR loss of 3 dB is considered. Note that this is a significant loss as it represents the average SNR loss for all satellites per pseudolite signal. Initially a conservative estimate is made based on the small signal approximation of (43). This estimate is conservative for low duty cycles as it ingores the impact of saturation. For higher duty cycles, on the other hand, the small signal approximation becomes invalid, since the AGC response will be greatly affected by the pseudolite signal itself. The minimum distance required to ensure the maximum SNR loss threshold is met is found by solving (43) (ignoring the quantization loss) to obtain the effective C/N_0, then inverting (68) to obtain the required distance.

Fig. 17 shows the results of computing the minimum distance for GPS signals with the effective transmit powers defined above. Note that under the small signal approximation the loss distance is the same for all duty cycles. This is due to the fact that it is assumed that the *effective* transmit power is the same for all duty cycles, thus the effective C/N_0 is the same for all duty cycles at a given distance. In reality there are two factors that cause divergence from the predictions of the small signal model:

1. For low pulse duty cycles as the ADC starts to saturate the minimum distance will reduce
2. For longer pulse duty cycles as the ADC becomes “captured” by the pseudolite signal, the minimum distance will increase.

The former effect can be approximated by considering the sigmoidal approximation to the SNR loss. Fig. 18 shows the results of applying the sigmoidal interpolation approximation to the loss model, and inverting the result for a desired loss of 3 dB and computing the corresponding distance for a given effective transmit power. Two approximations are made, one based on the Javad GPS receiver data, the other based on the u-Blox data. Note that in both cases the minimum distance decreases as the duty cycle approaches a certain minimum value. This minimum duty cycle is that value for which the saturation loss is equal to the loss threshold. If the duty cycle is lower than this minimum value then the loss threshold will never be exceeded, no matter how close the transmitter and receiver become.

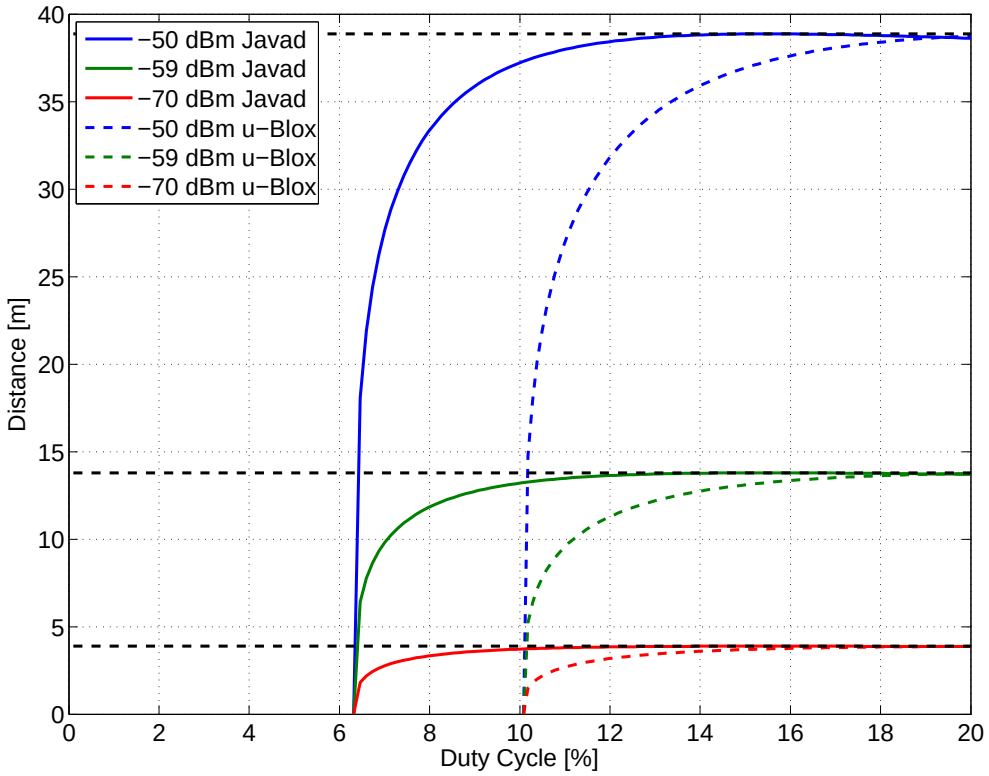

Figure 18: Minimum distance vs duty cycle for GPS C/A code signals under the sigmoidal interpolation approximation. SNR loss threshold = 3 dB. The loss distances under the small signal approximation are indicated with black dashed lines.

Fig. 19 shows the same results but for the case of the Javad Galileo data. The Galileo receiver is less sensitive to the effects of the GPS pseudolite than either of the two GPS receivers. This is due to the increased SSC between the pseudolite and local replica signals. The result is that the Galileo receiver can come closer to the pseudolite before reaching the SNR threshold, and has a higher minimum duty cycle requirement. Of course, this situation would be reversed if the SSC between the pseudolite signal and the local replica was greater for Galileo than for GPS signals.

5.2 1 dB SNR Loss Threshold

In this section a maximum allowable SNR loss of 1 dB is considered. This may be a more realistic threshold to set in practice. Fig. 20 shows the predicted minimum distance for the two GPS receivers under consideration based on the sigmoidal approximation. Again, it can be seen that, for a sufficiently low duty cycle the SNR loss never reaches the threshold. At larger duty cycles, the saturation loss is greater than the threshold and the minimum distance approaches that for the continuous pseudolite. Fig. 21 shows the same results for the Javad Galileo receiver. Again, this receiver is less sensitive to the GPS pseudolite, due to the increased spectral separation between the pseudolite and local replica signals. For this 1 dB threshold it is interesting to note that the minimum duty cycles are all low ($< 10\%$), implying that this threshold is, in practice, likely to be met for some minimum distance.

The above plots are useful for determining the appropriate duty cycle for a given application. The effective transmit power level determines the maximum achievable performance of the pseudolite-enabled receiver, thus the pseudolite performance is constant along the curves. Clearly lower duty cycles result in reduced minimum distances, or equivalently reduced SNR losses for a given distance. On the other hand, reducing the duty cycle leads to an increase in the peak power level, which may be detrimental to other shared services [4], and may also require longer integration times in the participating receiver [15]. These aspects of pulsing may require further study on a case-by-case basis.

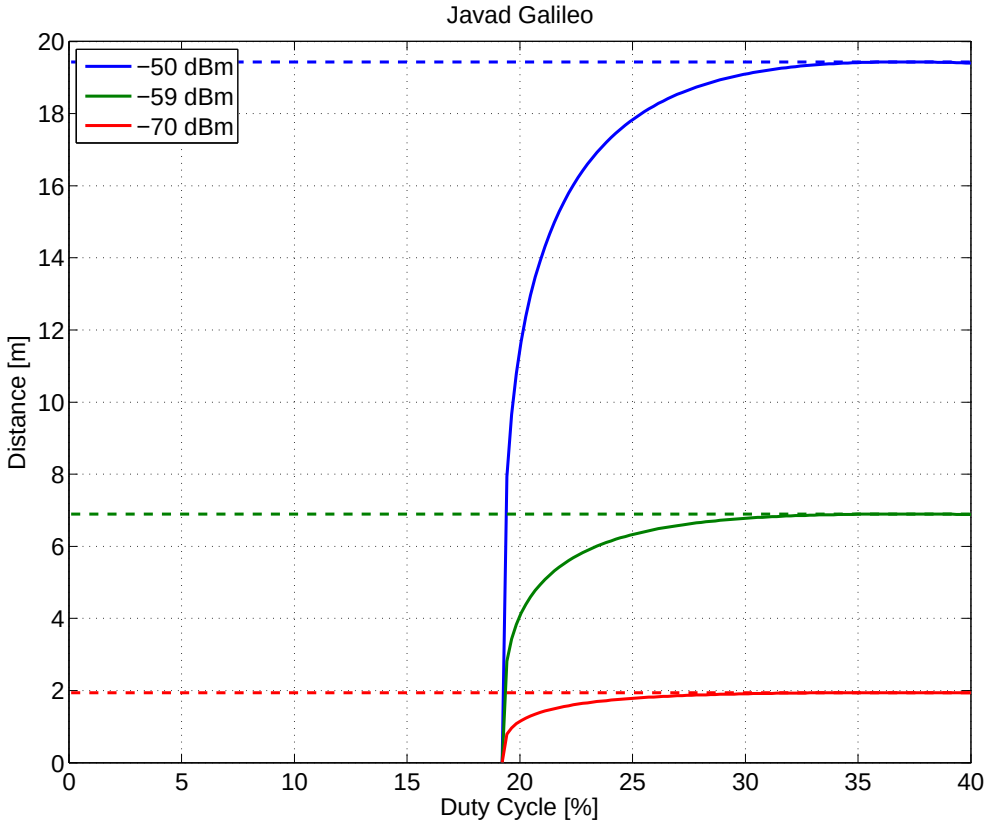

Figure 19: Minimum distance vs duty cycle for Galileo E1b/c signals under the sigmoidal interpolation approximation. SNR loss threshold = 3 dB. The loss distances under the small signal approximation are indicated with dashed lines.

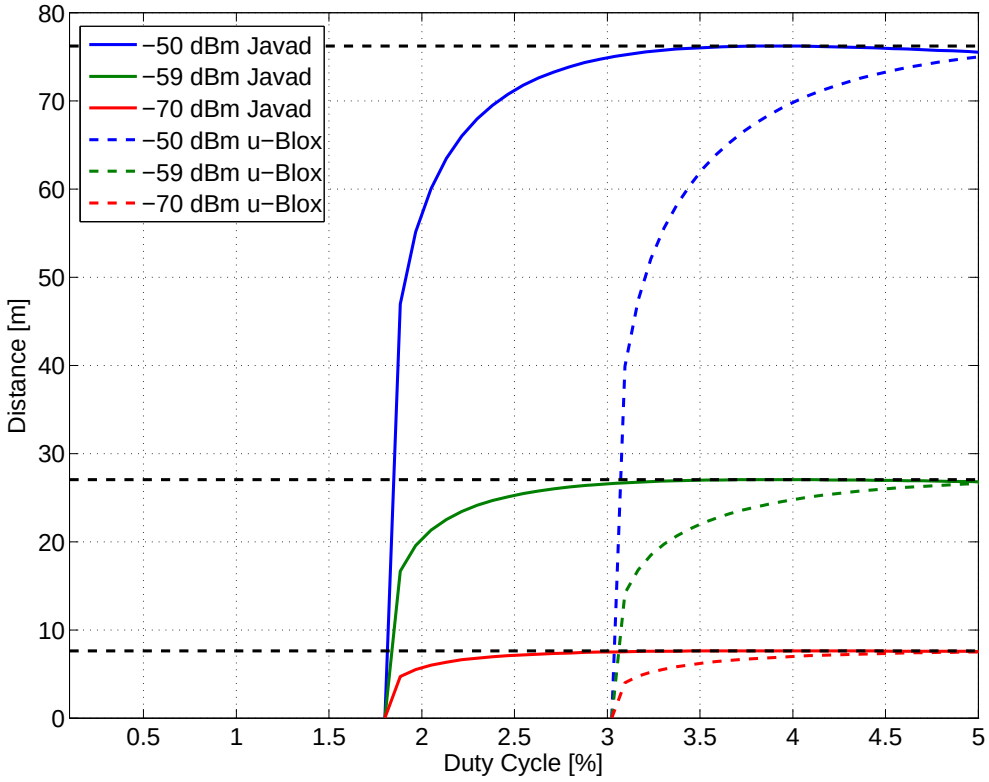

Figure 20: Minimum distance vs duty cycle for GPS C/A code signals under the sigmoidal interpolation approximation. SNR loss threshold = 1 dB. The loss distances under the small signal approximation are indicated with black dashed lines.

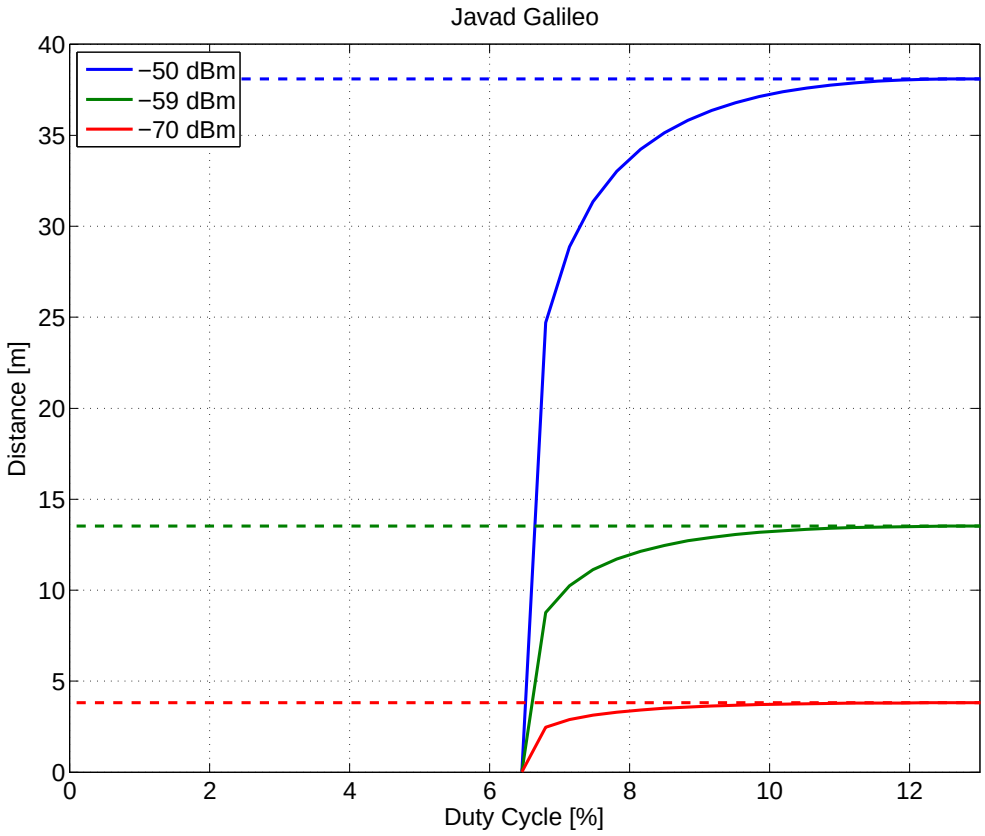

Figure 21: Minimum distance vs duty cycle for Galileo E1b/c signals under the sigmoidal interpolation approximation. SNR loss threshold = 1 dB. The loss distances under the small signal approximation are indicated with dashed lines.

6 Conclusion and Recommendations

In this report a two-part model of the impact of pseudolites on non-participating GNSS receivers has been developed. The two regions of applicability are:

1. The small signal approximation - when the pseudolite signal is below the noise floor
2. Saturation - when the pseudolite saturates the receiver's ADC.

In addition, a simple sigmoidal approximation has been proposed to interpolate between the two regions. The model has been verified using data collected from two commercial GPS receivers, a wide-band high-precision receiver and a narrow-band commercial receiver. The high-precision receiver was also capable of processing Galileo signals. The impact of the spectral separation between the pseudolite signal and the locally replica in the receiver was clearly demonstrated by the fact that the Galileo signals suffered less SNR degradation then the GPS signals in the presence of a GPS pseudolite. In addition, the wide-band high-precision receiver suffered greater losses than the narrow-band commercial receiver, as predicted by the model.

Based on model parameters extracted from the experimental data, a number of case studies were considered. For each test case a minimum distance was computed, such that a non-participating receiver further away from the pseudolite than this minimum distance should experience average C/N_0 losses less than a given threshold. For the worst case considered, corresponding to an effective transmit power of -50 dBm and the high-precision GPS receiver, a minimum distance of ~ 75 m is required to ensure an induced SNR loss of less than 1 dB. This minimum distance can be reduced only by reducing either the transmit power, or the duty cycle or both. For example, keeping the effective transmit power constant the duty cycle would need to be reduced to less than 2% to bring the minimum distance below 30 m. On the other hand, if the effective transmit power was reduced -59 dBm the corresponding minimum distance is at most ~ 28 m.

In conclusion, the proposed model provides a mechanism for determining the impact of transmit power levels and duty cycle on non-participating receivers. This analysis can be used in conjunction with experimentally or theoretically derived parameters to determine recommendations for pseudolite systems. For any deployed system it will be important to consider the worst case performance of non-participating receivers, meaning those receivers with largest bandwidth and/or greatest bit resolution that are likely to be active in the vicinity of the pseudolites. Further analysis would also be required to determine the impact of any proposed system on other shared services and the practical performance of participating receivers. For example, it has been assumed herein that the participating receiver can optimally process the pseudolite signals, fully exploiting the effective pseudolite C/N_0. In practice this ability may be limited by the receiver's dynamic range and the speed of response of its AGC.

References

[1] José Ángel Ávila Rodrguez. *On Generalized Signal Waveforms for Satellite Navigation*. Phd thesis, University FAF Munich, June 2008.

[2] Stewart H. Cobb. *GPS pseudolites: Theory, Design and Applications*. Phd thesis, Stanford University, September 1997.

[3] Cillian O'Driscoll, Daniele Borio, and Joaquim Fortuny. Scoping study on pseudolites. Technical report, EC Joint Reseach Centre, March 2011.

[4] Electronic Communications Committee (ECC). Compatibility studies between pseudolites and services in the frequency bands 1164-1215, 1215-1300 and 1559-1610 MHz. Technical report, European Conference of Postal and Telecommunications Administrations (CEPT), Dublin, January 2009.

[5] Daniele Borio and Joaquim Fortuny. Impact of pseudolite signals on non-participating GPS receivers: Compatibility analysis for commercial receivers. Technical report, EC Joint Reseach Centre, November 2010.

[6] Thomas A. Stansell. RTCM SC-104 recommended pseudolite signal specification. *NAVIGATION: Journal of The Institute of Navigation*, 33(1):42–59, Spring 1986.

[7] John W. Betz. The offset carrier modulation for gps modernization. In *Proc. of the 1999 National Technical Meeting of The Institute of Navigation*, pages 639–648, San Diego, CA, January 1999.

[8] E. D. Kaplan and C. Hegarty, editors. *Understanding GPS: Principles and Applications*. Artech House Publishers, 2nd edition, November 2005.

[9] John W. Betz. Effect of partial-band interference on receiver estimation of C/N_0. In *Proc. of the 2001 National Technical Meeting of The Institute of Navigation*, pages 817 – 828, Long Beach, CA, January 2001.

[10] J. W. Betz. Effect of narrowband interference on GPS code tracking accuracy. In *Proc. of ION National Technical Meeting*, pages 16–27, Anaheim, CA, January 2000.

[11] Daniele Borio. *A statistical theory for GNSS signal acquisition*. Phd thesis, Politecnico di Torino, April 2008.

[12] R. Price. A useful theorem for nonlinear devices having gaussian inputs. *Information Theory, IRE Transactions on*, 4(2):69 –72, june 1958.

[13] A. J. Van Dierendonck, Pat Fenton, and Chris Hegarty. Proposed airport pseudolite signal specification for GPS precision approach local area augmentation systems. In *Proceedings of the Internation Technical Meeting of the Satellite Division of the Institute of Navigation (ION GPS 97)*, Kansas, MI, September 1997.

[14] Electronic Communications Committee (ECC). Regulatory framework for indoor GNSS pseudolites. Technical Report ECC Report 168, European Conference of Postal and Telecommunications Administrations (CEPT), Miesbach, May 2011.

[15] Cillian O'Driscoll, Daniele Borio, and Joaquim Fortuny-Gausch. Investigation of pulsing schemes for pseudolite applications. In *Proceedings of the 24th International Technical Meeting of the Satellite Division of the Insititute of Navigation (ION GNSS 2011)*, Portland, OR, 19–23 September 2011.

European Union

EUR xxxxx EN- Joint Research Centre - Institute for the Protection and Security of the Citizen
Impact of Pseudolite Signals on Non-Participating GNSS Receivers
D. Borio, C. O'Driscoll, J. Fortuny
Luxembourg: Publications Office of the European Union
2010-
EUR - Scientific and Technical Research series - ISSN 1018-5593
ISBN X-XXXX-XXXX-X
DOI XXXXX

Abstract
Pseudo-satellites or pseudolites are ground based-transmitters designed for location applications and expected to play the role of GNSS satellites when GNSS signals are not available or do not provide sufficient coverage/accuracy. Although pseudolites have the potential to bridge the gap between outdoor and indoor location, compatibility issues can arise with existing GNSS systems. More specifically, pseudolite signals can interfere with existing GNSS modulations and degrade the performance of non-participating receivers (receivers not designed to handle pseudolite signals).
In this report, a theoretical framework able to approximately predict the loss caused by a pseudolite signal on a non-participating receiver is developed. The model is supported by experimental findings obtained by testing commercial GNSS receivers. Finally, the proposed model, tuned according to the experimental findings, has been used to determine minimum distances and maximum duty cycles that should be adopted in order to limit to a predefined value the loss in GNSS signal quality .
This report is intended as a contribution for the compatibility analysis between pseudolites and GNSS performed by CEPT.

The mission of the JRC is to provide customer-driven scientific and technical support for the conception, development, implementation and monitoring of EU policies. As a service of the European Commission, the JRC functions as a reference centre of science and technology for the Union. Close to the policy-making process, it serves the common interest of the Member States, while being independent of special interests, whether private or national.